Article

Cell

Cross-talk between Lysine-Modifying Enzymes Controls Site-Specific DNA Amplifications

Graphical Abstract

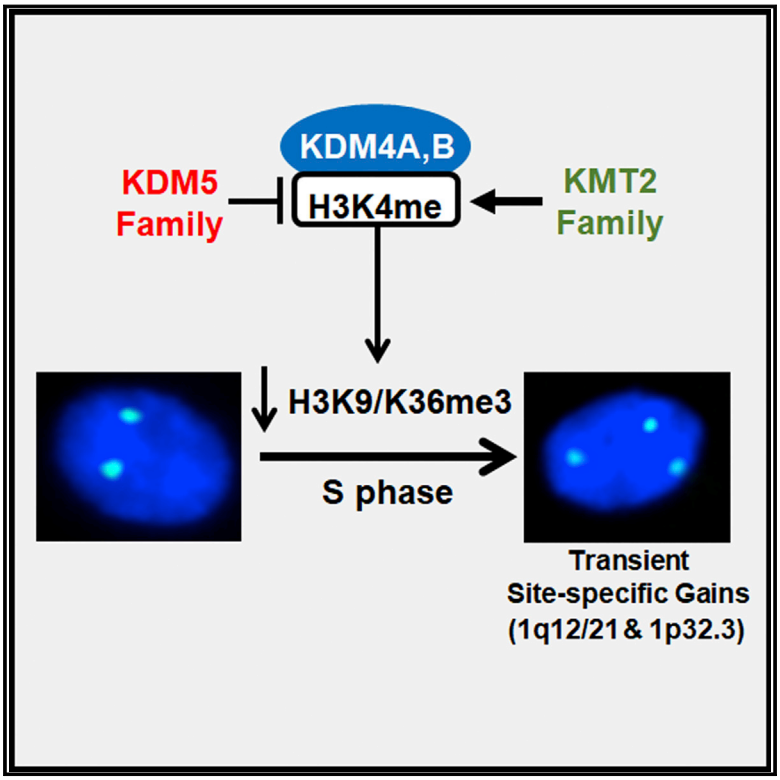

Authors

Sweta Mishra, Capucine Van Rechem, Sangita Pal, ..., Michael S. Lawrence, Danette L. Daniels, Johnathan R. Whetstine

Correspondence

jwhetstine@hms.harvard.edu

In Brief

Histone lysine methyltransferases and demethylases collaborate to promote site-specific DNA copy number gains.

Highlights

- Histone lysine methylation dynamics control site-specific DNA amplification
- H3K4 methylation balance regulates KDM4A targeting to copy gained sites
- A lysine methyltransferase-demethylase network directs KDM4A-independent copy gain
- H3K36 methylation controls site-specific copy gains independent of H3K9 methylation

Mishra et al., 2018, Cell *174*, 803–817
August 9, 2018
https://doi.org/10.1016/j.cell.2018.06.018

CellPress

Cell

Cross-talk between Lysine-Modifying Enzymes Controls Site-Specific DNA Amplifications

Sweta Mishra,[1] Capucine Van Rechem,[1,5] Sangita Pal,[1] Thomas L. Clarke,[1] Damayanti Chakraborty,[1] Sarah D. Mahan,[2] Joshua C. Black,[1,6] Sedona E. Murphy,[1,7] Michael S. Lawrence,[3,4] Danette L. Daniels,[2] and Johnathan R. Whetstine[1,8,*]

[1]Massachusetts General Hospital Cancer Center and Department of Medicine, Harvard Medical School, 13th Street, Charlestown, MA 02129, USA

[2]Promega Corporation, 2800 Woods Hollow Road, Madison, WI 53711, USA

[3]Massachusetts General Hospital Cancer Center and Department of Pathology, Harvard Medical School, 13th Street, Charlestown, MA 02129, USA

[4]Broad Institute of Harvard and MIT, 415 Main Street, Cambridge, MA 02142, USA

[5]Present address: Stanford Medicine, Department of Pathology, 269 Campus Drive, Stanford, CA 94305, USA

[6]Present address: University of Colorado School of Medicine Anschutz Medical Campus, Department of Pharmacology, 12800 E. 19th Avenue, Aurora, CO 80045, USA

[7]Present Address: Stanford Medicine, Department of Genetics and Developmental Biology, 279 Campus Drive, Stanford, CA 94305, USA

[8]Lead Contact

*Correspondence: jwhetstine@hms.harvard.edu

https://doi.org/10.1016/j.cell.2018.06.018

SUMMARY

Acquired chromosomal DNA amplifications are features of many tumors. Although overexpression and stabilization of the histone H3 lysine 9/36 (H3K9/36) tri-demethylase KDM4A generates transient site-specific copy number gains (TSSGs), additional mechanisms directly controlling site-specific DNA copy gains are not well defined. In this study, we uncover a collection of H3K4-modifying chromatin regulators that function with H3K9 and H3K36 regulators to orchestrate TSSGs. Specifically, the H3K4 tri-demethylase KDM5A and specific COMPASS/KMT2 H3K4 methyltransferases modulate different TSSG loci through H3K4 methylation states and KDM4A recruitment. Furthermore, a distinct chromatin modifier network, MLL1-KDM4B-KDM5B, controls copy number regulation at a specific genomic locus in a KDM4A-independent manner. These pathways comprise an epigenetic addressing system for defining site-specific DNA rereplication and amplifications.

INTRODUCTION

Cancer cells have multiple chromosomal aberrations. Genome-wide studies of somatic copy number alterations (SCNAs) across multiple different tumor types have demonstrated that specific chromosomal regions exhibit higher frequencies of DNA copy number gains and amplifications, with a concomitant increase in the associated gene expression (Beroukhim et al., 2010; Kim et al., 2013; Zack et al., 2013). These regions frequently harbor pro-survival genes and oncogenes. For example, the gain of chromosome 1q12-25 (chr 1q12-25) are associated with a number of drug resistance-associated oncogenes (e.g., *MCL1*, *CKS1B*; [Beroukhim et al., 2010; Diskin et al., 2009; Fonseca et al., 2006; Inoue et al., 2004; Kudoh et al., 1999; Petersen et al., 2000]). Drug selection can also result in the appearance of integrated or extrachromosomal gene amplification as seen for *dihydrofolate reductase* (*DHFR*) when cells are treated with methotrexate (Alt et al., 1978; Biedler and Spengler, 1976a, 1976b; Haber and Schimke, 1981) or the loss of extrachromosomal fragments for *epidermal growth factor receptor* (*EGFR*) gene amplifications in glioblastoma patients (Nathanson et al., 2014). A recent study illustrated that ~50% of the evaluated tumors contain extrachromosomal amplifications that impact tumor heterogeneity and help in tumor adaptation (Turner et al., 2017). Even though DNA copy gains are frequent in cancer, little knowledge exists about the mechanisms that generate site-specific DNA copy gains *de novo* or under selective pressure.

Previously, overexpression and stabilization of histone 3 lysine 9/36 (H3K9/36) tri-demethylase KDM4A, as well as the direct modulation of chromatin states (i.e., H3K9 and K36 methylation), resulted in site-specific DNA copy gains of drug-resistance-associated loci without causing genome-wide chromosomal instability (i.e., chr 1q12h, 1q21.2, 1q21.3). These DNA copy gains were extrachromosomal, occurred during S phase, and were lost in late S/early G2 phase of the cell cycle (Black et al., 2013, 2015, 2016). The transient behavior of the KDM4A-dependent DNA copy gains highlights the inherent plasticity that these epigenetic factors could confer to regions that undergo amplification. This discovery emphasized that a single chromatin factor modulated transient site-specific copy gains (TSSGs) (Mishra and Whetstine, 2016). However, this initial study did not address whether additional chromatin factors or their associated histone methylation states control TSSG formation. Furthermore, it remained unclear how KDM4A is targeted or whether additional mechanisms control TSSG formation independent of KDM4A. Answering these outstanding questions will expand our understanding about the regulation and impact of site-specific copy gains and identify mechanisms contributing to pathological DNA amplifications.

This study begins to address how chromatin modulators and their associated histone modification states impact site-specific

rereplication and DNA copy gains. By conducting an unbiased small interfering RNA (siRNA) screen for lysine demethylases (KDMs), a role for the H3K4 tri-demethylase KDM5A in restricting TSSGs was identified. KDM5A depletion and increased H3K4me3 serve as beacons for KDM4A recruitment and the associated amplifications. Furthermore, a cross-talk between specific MLL/COMPASS H3K4 methyltransferases, KDM5A and KDM4A at subsets of TSSGs was discovered. In addition, a KDM4A-independent TSSG site was uncovered. This TSSG was regulated by an intricate interplay between KMT2A/MLL1, KDM5B, and KDM4B. These findings highlight a key role for H3K4 methylation in regulating TSSGs while illustrating a more generalizable role for chromatin modifiers and localized epigenetic states in controlling rereplication and DNA amplification.

RESULTS

KDM5A Depletion Promotes Site-Specific Copy Gains

Our laboratory demonstrated that histone lysine demethylase KDM4A generated TSSGs of regions on chromosomes 1 and X (Black et al., 2013). These loci have been linked to drug resistance and poor patient outcome (Fonseca et al., 2006; Inoue et al., 2004; Kudoh et al., 1999). In fact, the chromosome 1q12h region has been observed as an enriched region across several tumor types upon KDM4A amplification (Black et al., 2013). Using the TCGA pan-cancer dataset (7,885 samples) obtained from the TCGA GDAC (Zack et al., 2013), we measured the percentage of samples carrying an amplification ($\geq$2.4 copies) in each of the loci on chromosome 1 associated with TSSGs. We also measured *EGFR* and *MYC* as representatives of frequently amplified cancer driver genes (Table S1). These data illustrate that amplification of these genomic regions occurs frequently in tumors (e.g., 21% for 1q21.3 compared to 26% for *MYC* in liver cancer), which raises the possibility that additional chromatin factors control their copy gains. Therefore, we conducted an unbiased siRNA screen against all lysine demethylase families (KDM1–KDM7) (Figure 1A). These were performed in immortalized retinal pigment epithelial cells (RPEs) that have a nearly diploid genome (Black et al., 2013; Jiang et al., 1999). Each independent set of siRNAs was validated and assessed for major cell cycle defects by flow cytometry analysis before being assayed by DNA fluorescence *in situ* hybridization (DNA FISH) (Figures S1A–S1Q).

Evaluation of FACS profiles revealed that several KDMs resulted in modest yet significant changes in cell cycle distribution (Figures S1K–S1Q). For all KDM siRNA samples, we initiated the TSSG screen with a FISH probe against a well-characterized locus (chromosome 1q12h; referred to as 1q12h) that has been used to elucidate TSSG events in cancer cells (Black et al., 2013, 2015, 2016). We also included another probe that did not undergo TSSG across a panel of experimental conditions, serving as a negative control region (chromosome 8 centromere, 8c) (Figures 1B, 1C, and S1R–S1W). Positive hits for 1q12h DNA copy gain were then screened against a panel of other TSSG sites and additional chromosome 1 regions that had not been observed to undergo copy gains by DNA FISH (e.g., 1q23.3 was used for all conditions throughout the paper; Table S2) (Black et al., 2013, 2015, 2016). This approach ensures TSSG site-specificity versus global instability. For all FISH probes, we have plotted the data as percentages of copy gains per probe per cell instead of a ratio against a selected control region such as 1q23.3. This method allows one to see the specificity for copy changes while appreciating baseline copy number levels for regions being FISHed within and across chromosomes (Møller et al., 2018) and also ensures that we can detect copy number changes at centromeric regions that would be otherwise lost through normalization.

From our screen, only the depletion of KDM5A caused a significant increase in 1q12h copy gains, while 8c showed no significant changes (Figures 1B, 1C, S1I, and S1O). The 1q12h copy gains were further validated with cells depleted with independent shRNAs targeting KDM5A (Figures S1X and S1Y). Furthermore, spectral karyotyping (SKY) of KDM5A depleted cells showed no major karyotype issues (data not shown). These results were not cell type dependent, as H2591 lung cancer cells also exhibited 1q12h copy gain upon KDM5A depletion (Figure 1D and Figures S1Z–S1A'). KDM5A depletion was also sufficient to cause other previously identified TSSGs to undergo copy number gains (i.e., 1q21.2 and Xq13.1), while additional regions on chromosome 1 and X (i.e., 1q23.3, 1qTel, Xcen) remained unaffected (Figure 1E and Table S2).

To further assess the role of KDM5A depletion, we applied chemical inhibition to assess TSSG formation (KDM5i, KDM5-C70 [Johansson et al., 2016]) (Figures 1F–1G and S1B'–S1D'). KDM5i treatment caused a global increase in H3K4me3 level, as observed previously (Figure S1C'). Furthermore, KDM5i caused a dose-dependent increase in 1q12h copy gains in multiple cell lines (Figures 1F, 1G, S1B', and S1D'). Consistent with the requirement for KDM5A in regulating TSSGs, chromatin immunoprecipitation (ChIP) analyses demonstrated a significant reduction of KDM5A at TSSG sites upon KDM5A siRNA treatment (Figure 1H), which suggests that KDM5A directly binds to these regions to suppress copy number gains.

KDM5A-Dependent Copy Gains Are Transient, Require S Phase, and Are Derived from Rereplication

TSSGs are transient and occur in an S-phase-dependent manner (Black et al., 2013). To determine whether KDM5A-dependent gains were transient, we washed off KDM5i and assessed TSSGs (Figure 2A). RPE cells generated copy gains after 48 or 72 hr of KDM5i treatment (no wash off); however, DNA copy gains were significantly diminished after the drug was removed (24 hr wash off, Figures 2B, 2C, and S2A). Consistent with these observations, extra copies were not observed on mitotic chromosomes after KDM5i treatment (i.e., 1q12h; Figure S2B). These experiments highlight the transient nature of the KDM5A-dependent copy gains.

In order to determine whether the copy gains are generated during S phase, RPE cells were arrested in G1/S with hydroxyurea (HU) treatment before receiving KDM5i (Figure 2D). The pretreatment with HU blocked KDM5i from generating DNA copy gains (Figures 2E and S2C). However, KDM5i-treated cells released from HU generated copy gains (Figures 2F and S2C), demonstrating that KDM5i results in S-phase-dependent copy gains.

Rereplication is one mechanism underlying TSSG generation (Black et al., 2013). In order to determine whether depletion of KDM5A induced rereplication, we first performed cesium

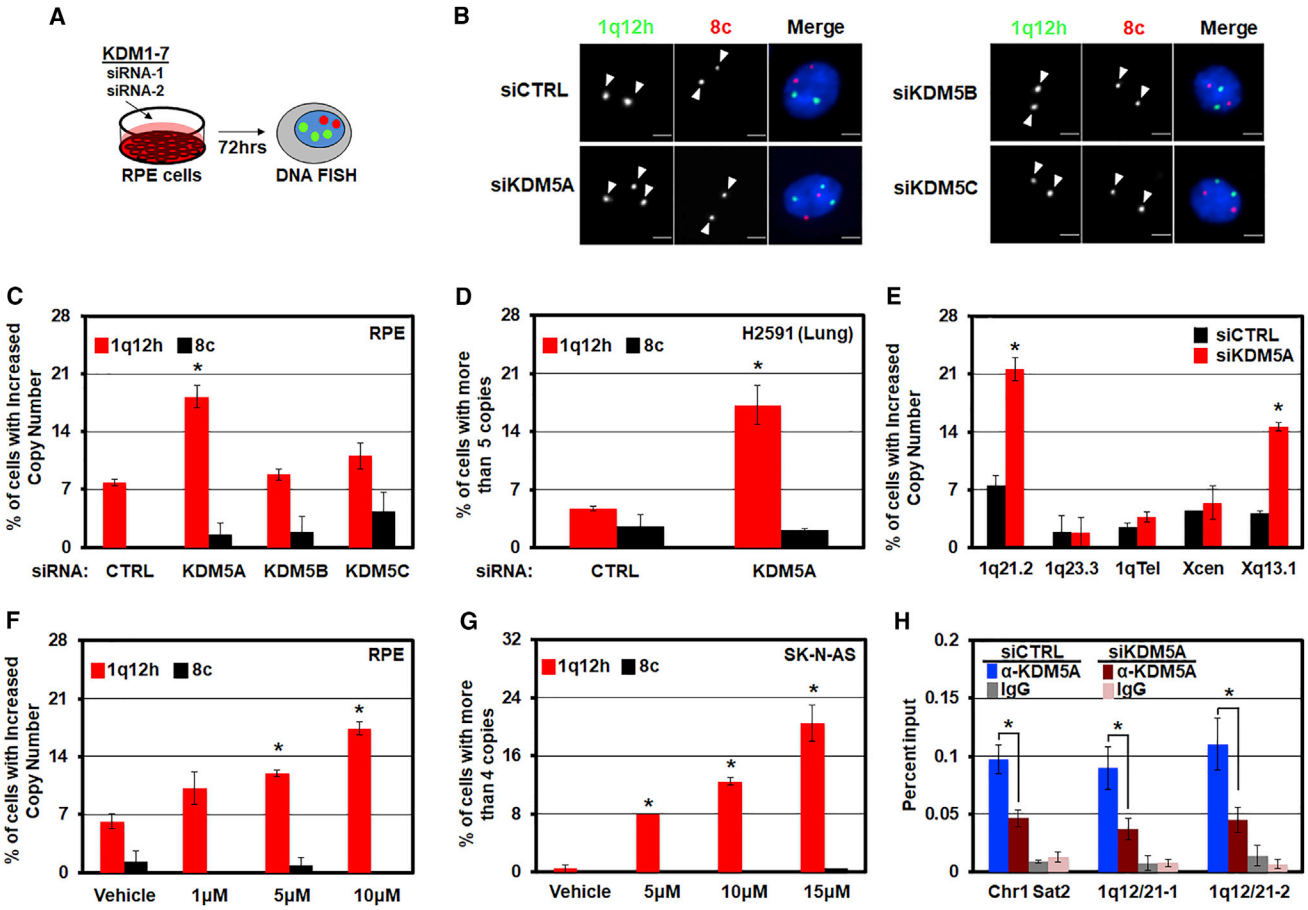

Figure 1. KDM5A Inhibition Promotes Site-Specific Copy Gains

(A) A schematic of siRNA screen in RPE cells against KDM1 through KDM7 family members.
(B) Representative DNA FISH images for the indicated KDM5 family siRNAs for chromosome 1q12h (green), 8c (red), and merged with DAPI (blue) are shown.
(C) Only KDM5A depletion caused 1q12h copy gains in RPE cells.
(D) KDM5A knockdown results in site-specific copy gains in H2591 cells.
(E) KDM5A knockdown results in site-specific copy gains of additional regions in RPE cells.
(F) Quantification of FISH in RPE cells treated with increasing doses of KDM5i (KDM5-C70).
(G) Quantification of FISH in SK-N-AS cells treated with increasing doses of KDM5i.
(H) KDM5A occupancy at copy gained regions upon siRNA depletion are shown.
Error bars represent the SEM. *$p < 0.05$ by two-tailed Student's t test. Scale bar, 5 μm.

chloride density gradient ultracentrifugation to isolate rereplicated DNA (termed heavy-heavy, H:H; Figures 2G and S2D) for both control and KDM5A knockdown cells. The heavy-heavy fractions for each cellular condition were pooled together before the genomic DNA was purified and quantified by polymerase chain reaction (qPCR) (Figure 2G). We observed significant enrichment of heavy-heavy DNA at copy gained regions 1q12h, 1q12/21, 1q21.2, and Xq13.1 upon KDM5A depletion (Figure 2H); however, no enrichment was observed at the 1q23.3 control region. This suggested that reduced KDM5A levels promote rereplication at sites undergoing TSSG.

KDM5A Depletion Promotes TSSG Generation Post S Phase

TSSGs generated by KDM4A overexpression are cleared by the end of S phase and beginning of G2 phase of the cell cycle (Black et al., 2013). Therefore, we tested whether the copy gains generated by KDM5A depletion follow the same kinetics. The cells were arrested in late G2 with a CDK1 inhibitor (CDK1i, Ro-3306) before copy gain was analyzed by DNA FISH (Figure 2I). We observed that the TSSGs generated by KDM5A depletion occurred after Ro-3306 treatment (Figures 2J, S2E, and S2F), which demonstrated that copy gains occurred or persisted outside of S phase. Therefore, either the mechanism(s) that remove copy number gains are altered in KDM5A depleted cells, or the copy gains are still being generated during the G2 phase of the cell cycle in KDM5A depleted cells. Since these copy gains were transient, we hypothesized that KDM5A depletion created a permissive chromatin state that allowed replication to occur during late G2. To test this possibility, we determined whether DNA polymerase (i.e., DNA Polα) was present during late G2 at rereplicated regions. Upon KDM5A depletion, cells arrested in

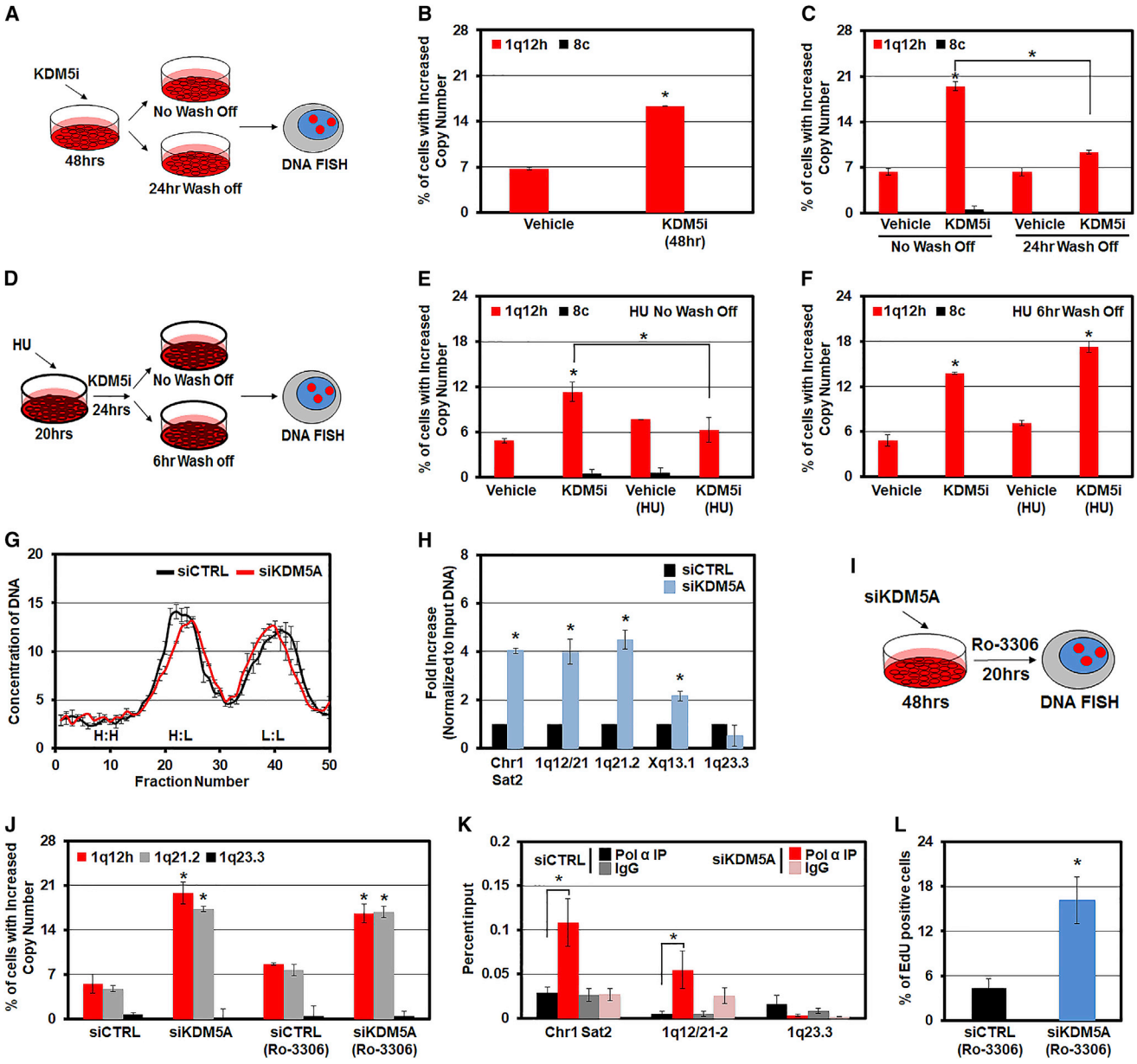

Figure 2. KDM5A-Associated Site-Specific Copy Gains Are Transient, Require S Phase, and Are Rereplicated

(A) A schematic of KDM5i treatment conditions are shown for (B) and (C).

(B and C) Quantification of FISH with KDM5i (B) and upon wash off (C).

(D) A schematic of drug treatment conditions is shown for (E) and (F).

(E) KDM5i after HU arrest does not result in copy gains.

(F) Copy gains are restored upon HU release.

(G) A graph for the heavy-heavy (H:H), heavy-light (H:L) and light-light (L:L) peaks from the cesium chloride density gradient centrifugation fractions.

(H) qPCR graph of pooled heavy-heavy DNA (H:H) is shown, which plots the fold change in rereplication.

(I) Schematic for Ro-3306 treatment.

(J) Copy gains persisted after siKDM5A and Ro-3306 treatment.

(K) DNA Polymerase alpha (Pol α) ChIP in siRNA and Ro-3306 treated cells are shown.

(L) Quantification of EdU positive cells after Ro-3306 treatment from control and KDM5A knockdown cells.

Error bars represent the SEM. *$p < 0.05$ by two-tailed Student's t test.

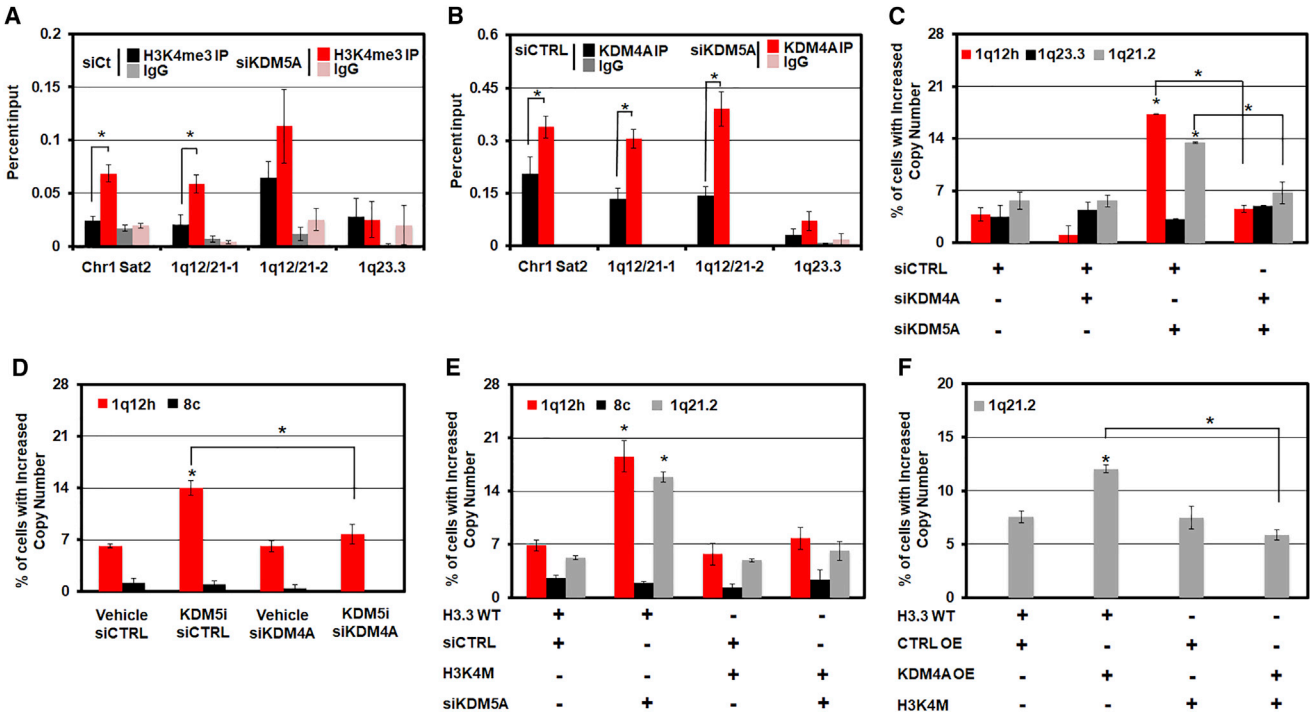

Figure 3. KDM5A Depletion Promotes H3K4me3 and KDM4A Recruitment at Copy-Gained Loci

(A) H3K4me3 ChIP in control and KDM5A knockdown cells.

(B) KDM4A ChIP in control and KDM5A knockdown cells.

(C) DNA FISH after co-depletion of KDM4A and KDM5A.

(D) KDM4A depletion rescued KDM5i mediated copy gain (i.e., 1q12h).

(E) DNA FISH after histone H3.3 lysine 4 to methionine (H3K4M) transduction in siRNA depleted cells.

(F) DNA FISH after transduction with H3K4M in KDM4A overexpressing cells (KDM4A OE).

Error bars represent the SEM. *p < 0.05 by two-tailed Student's t test.

late G2 had enriched DNA Polα occupancy at rereplicated and copy-gained loci compared to control cells, while a non-copy-gained locus did not have DNA Polα enrichment (Figure 2K). Furthermore, we observed significant enrichment of EdU in late G2 upon KDM5A depletion, which suggested that DNA synthesis occurred during late G2 arrest (Figures 2L, S2G, and S2H). Taken together, our observations support the hypothesis that KDM5A depletion alters the chromatin state so that rereplication and copy gains occur during S phase and continues into late G2, which is consistent with a previous report suggesting that KDM5A impacts origin recognition (Huang et al., 2016).

KDM5A-Dependent Copy Gains Require KDM4A

KDM5A demethylates H3K4me3/2/1 and associates with reduced gene expression (Christensen et al., 2007; Iwase et al., 2007; Klose et al., 2007). Therefore, KDM5A depletion could promote KDM4A overexpression and, in turn, cause TSSGs as previously shown (Black et al., 2013). However, KDM4A protein levels did not change upon KDM5A depletion (Figure S3A). Since the Tudor domains within KDM4A recognize H3K4me3 and H4K20me3 (Huang et al., 2006; Spektor and Rice, 2009) and are required for TSSGs (Black et al., 2013), we hypothesized that KDM5A depletion promotes DNA copy gains by increasing H3K4me3 and enriching KDM4A at rereplicated and DNA copy-gained sites. In fact, there were increased levels of H3K4me3 (Figures 3A and S3B) and KDM4A occupancy (Figure 3B) at regions undergoing amplification upon KDM5A depletion, but not within the non-copy-gained loci (1q23.3) (Figures 3A–3B and S3B). Therefore, we conducted DNA FISH on cells co-depleted for KDM4A and KDM5A or depleted for KDM4A and then treated with KDM5i (Figures S3C and S3D). Depletion of KDM4A blocked the DNA copy gains observed with either KDM5A depletion or KDM5i treatment (Figures 3C and 3D). In addition, the introduction of a histone H3.3 lysine 4 mutant (H3K4M) abrogated the TSSG generated by KDM5A depletion and KDM4A overexpression (Figures 3E–3F, S3E, and S3F). These observations illustrate a mechanism for recruiting KDM4A to sites that undergo site-specific rereplication and copy gains.

H3K4 KMTs Regulate Specific Sites Undergoing TSSG

Our results emphasized the importance of H3K4 methylation balance in regulating TSSGs. Therefore, we tested whether the H3K4 lysine methyltransferases (KMTs) regulate site-specific copy gains. Six H3K4 KMTs are part of the COMPASS family (MLL1/KMT2A, MLL2/KMT2B, MLL3/KMT2C, MLL4/KMT2D, SETD1A, and SETD1B; [Shilatifard, 2012]). Emerging evidence suggests that they have both overlapping and unique functions

in the genome through their roles in controlling K4 methylation states (Hu et al., 2013, 2017; Lee et al., 2013; Shilatifard, 2012).

First, KDM5A and KMT2 co-depletion experiments were conducted to identify the enzyme(s) balancing KDM5A modulation at TSSGs. The KMTs that rescued the TSSGs generated by KDM5A depletion were then assessed for their ability to generate TSSGs upon overexpression alone. By requiring the KMT to score in both assays, there was an increased probability that the enzyme was directly involved in modulating site-specific copy gains (Figure 4A).

The individual depletions and co-depletions for each KMT siRNA were verified for knockdown and assessed for major alterations in cell-cycle profiles by FACS (Figures S4A–S4M). Only minor, yet significant cell-cycle arrests were observed with KMT siRNAs. For example, SETD1A depletion alone resulted in an increase in G1/S, as previously reported (Figure S4L) (Tajima et al., 2015). We then evaluated copy gains upon the depletion of individual KMTs (Figures S4N–S4V). Only SETD1A depletion appeared to cause copy gains at most sites tested (Figure S4O, S4R, and S4U), which likely suggests global chromosomal instability in SETD1A-depleted cells. These data were consistent with SETD1A having key roles in modulating genome stability during cell division and by modulating DNA damage pathways (Hoshii et al., 2018; Tajima et al., 2015).

While independent KMT depletions did not cause site-specific gains, the depletion of select KMTs altered copy gains caused by KDM5A knockdown (Figures S4N–S4V). For example, depletion of KMT2B, KMT2C, KMT2D, and SETD1B rescued 1q12h and 1q21.2 copy gains caused by KDM5A depletion (Figures S4N–S4S). On the other hand, KMT2A/MLL1 and KMT2D/MLL4 depletion rescued 1q21.3 DNA copy gains (Figure S4T). These data suggest a higher degree of specificity for KMTs in generating site-specific DNA copy gains in the genome compared to KDMs. Since KMTs control the degree of methylation at specific locations in the genome (Hu et al., 2013, 2017; Lee et al., 2013; Shilatifard, 2012), the cross-talk between H3K4 KMTs (e.g., monomethyltransferases and trimethyltransferases) likely control the final methylation state and, in turn, the impact on TSSG formation. Therefore, the H3K4 methylation interplay between KMTs could explain why a collection of KMTs impacts certain TSSGs (e.g., 1q12h and 1q21.2).

To ensure that each KMT was truly regulating the sites undergoing TSSG, we overexpressed individual H3K4 KMTs except KMT2C because we could not generate a full-length expression vector. Overexpression was validated, and cells were FACS profiled (Figures S4W–S4B'). Upon overexpression, an even higher degree of specificity was observed for the KMTs than for the KDMs (Figures 4A and S4C'–S4N'). For example, SETD1B was the only KMT that generated 1q12h copy gains upon overexpression (Figures 4A and S4C'). The other KMTs did not generate 1q12h copy gains (Figures S4D'–S4F') even though some of them rescued the copy gains observed in KDM5A-depleted cells (Figures S4N–S4P). Consistent with the requirement for SETD1B catalytic activity to generate 1q12h, MDA-MB-231 breast cancer cells that had the SETD1B methyltransferase domain deleted (ΔSET domain [Wang et al., 2017]) were unable to generate 1q12h TSSGs upon KDM5A depletion (Figures S4O'–S4P'). In the case of 1q21.2, DNA copy gains were caused by KMT2B, KMT2D, and SETD1B (Figure S4G'–S4I'), while only KMT2A and KMT2D overexpression caused 1q21.3 DNA copy gains (Figure S4J'–S4M'). These observations illustrate that specific subsets of H3K4 KMTs are maintaining a balance with KDM5A at sites undergoing TSSG (Figure 4A).

Since KMT2 family members balance the TSSGs generated by KDM5A depletion and KDM4A was required for KDM5A-associated copy gains, we hypothesized that individual KMTs generate their associated TSSG via KDM4A. To test this hypothesis, we depleted KDM4A before overexpressing individual H3K4 KMTs (Figures 4B–4I and S5A–S5G). Since KMT2B expression was decreased after KDM4A depletion (Figure S5C), we did not assess the copy-gain relationship for this pair. However, TSSGs generated by overexpression of the other H3K4 KMTs were either completely or partially rescued upon KDM4A depletion (Figures 4B–4I). For example, depletion of KDM4A suppressed SETD1B generated 1q12h and 1q21.2 gains (Figures 4B–4C and 4E–4F) but only partially rescued 1q21.2 copy gains generated by KMT2D overexpression (Figure 4D). The 1q21.3 TSSG generated by either KMT2A or KMT2D overexpression was rescued upon KDM4A depletion (Figures 4G–4I). These data emphasize the need to balance KMT/KDM expression so that site-specific DNA amplification is kept in check.

Identification of a KDM4A-Independent TSSG

While testing whether KDM4A depletion could suppress each KMT-driven copy gain, we observed that KMT2A overexpression resulted in DNA copy gains at 1p32.3 (Figure 4G). This region did not copy gain with either KDM4A overexpression or KDM5A depletion (Figures 5A and 5B). Therefore, KMT2A overexpression generated a site-specific copy gain through another set of chromatin regulators.

We tested whether KDMs related to H3K4 could balance KMT2A-dependent DNA copy gains at 1p32.3. An siRNA screen against KDM5 family members identified KDM5B as a significant regulator of 1p32.3 DNA copy gains (Figures 5A and 5B). Consistent with this observation, shRNAs targeting independent sites within KDM5B also generated 1p32.3 copy gains (Figure S5H). Furthermore, chemical inhibition of the KDM5 family members generated copy gains of both 1p32.3 and 1q21.3 regions (Figure 5C). In order to determine if the 1p32.3 copy gains are transient, the KDM5i drug was washed off and the copy gains returned to baseline levels (Figures 5D and 5E). We did not observe extra 1p32.3 or 1p21.3 copies on metaphase spreads generated from KDM5i treated cells (Figure S5I). Collectively, these data suggest that the 1p32.3 copy gains are transiently generated.

We then demonstrated that KDM5B overexpression could block KMT2A-generated 1p32.3 copy gains (Figures 5F and S5J) without interfering with the other KMT2A copy-gained site (1q21.3) under KDM5A regulation (Figure 5F). The introduction of H3K4M also abrogated KDM5B- and KMT2A-dependent 1p32.3 copy gains (Figures 5G–5H, S3E, and S5K–S5M). In fact, H3K4M blocked both of the copy-gained regions generated by KMT2A (1p32.3 and 1q21.3) even though specific KDM5 members controlled these TSSGs. These data underscore an important role for H3K4 KMTs and KDMs in regulating TSSGs at other genomic loci that are independent of KDM4A regulation.

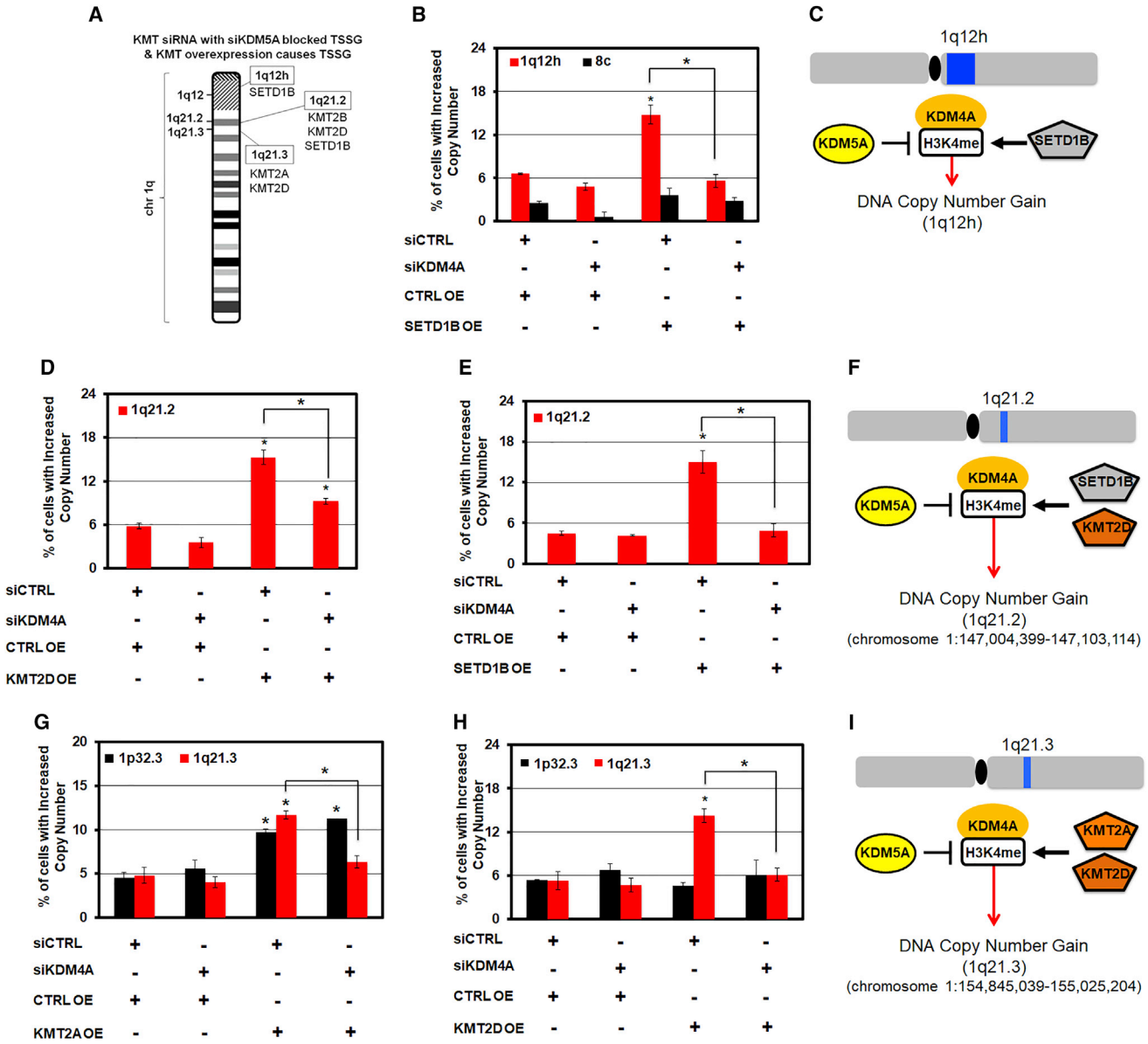

Figure 4. Site-Specific Copy Gains Are H3K4 KMT-Dependent

(A) A chromosome 1q arm ideogram summarizes the H3K4 KMTs that rescue copy gains caused by KDM5A depletion and that are generated upon KMT overexpression. DNA FISH data summarized in (A) can be found in Figure S4.

(B) KDM4A depletion followed by SETD1B overexpression blocked SETD1B-dependent 1q12h copy gains.

(C) A model depicting the interplay among KDM5A-KDM4A-SETD1B at 1q12h.

(D and E) KDM4A depletion followed by KMT2D (D) or SETD1B (E) overexpression abrogated 1q21.2 copy gains.

(F) A model summarizing the interplay of KDM5A-KDM4A-KMT2D and -SETD1B at the 1q21.2 locus.

(G) KDM4A depletion followed by KMT2A overexpression only abrogated 1q21.3 copy gains but not 1p32.3 copy gains caused by KMT2A overexpression.

(H) KDM4A depletion followed by KMT2D overexpression abrogated 1q21.3 copy gains.

(I) A Model illustrating the interplay among KDM5A-KDM4A-KMT2A and -KMT2D at the 1q21.3 locus. The locations are based on genome assembly GRCh37-hg19.

Error bars represent the SEM. *$p < 0.05$ by two-tailed Student's t test.

1p32.3 DNA Copy Gains Require KDM4B

Besides KDM4A, KDM4B and KDM4C also have Tudor domains that are involved in their recruitment to chromatin (Pedersen et al., 2016; Su et al., 2016). Therefore, we hypothesized that additional KDM4 enzymes could be involved in regulating 1p32.3 DNA copy gains. To test this hypothesis, we overexpressed KDM4A–C family members and assessed whether copy gains occurred at 1p32.3 locus. Only catalytically active

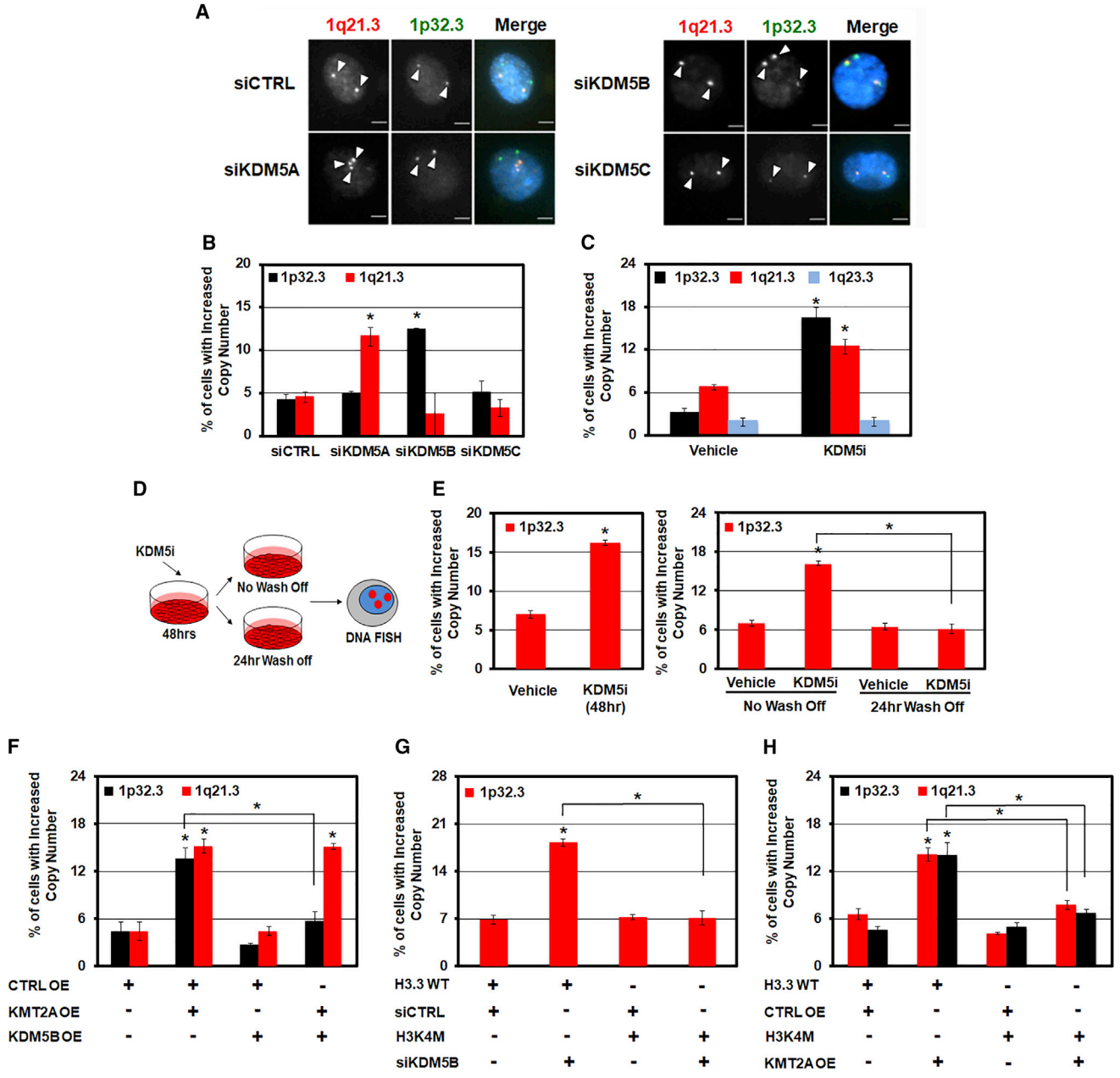

Figure 5. KDM5B Regulates the 1p32.3 TSSG

(A) Representative ilmages are shown for 1q21.3 (red), 1p32.3 (green) and DAPI (blue) merged after KDM5 family depletion.
(B) DNA FISH after KDM5 family depletion.
(C) 1p32.3 and 1q21.3 are copy gained after KDM5i.
(D) A schematic of KDM5i treatment.
(E) KDM5i treatment generated transient 1p32.3 copy gains.
(F) DNA FISH after co-overexpression of KMT2A and KDM5B.
(G) DNA FISH after H3K4M transduction followed by KDM5B siRNA depletion.
(H) H3K4M transduction blocked both 1p32.3 and 1q21.3 gains after KMT2A overexpression.
Error bars represent the SEM. *$p < 0.05$ by two-tailed Student's t test. Scale bar, 5 μm.

KDM4B overexpression resulted in significant 1p32.3 copy gains, while 1q12h, 1q21.3, and 1q23.3 loci remained unchanged (Figures 6A–6C and S6A–S6E). Furthermore, KDM4B overexpression promoted rereplication within the 1p32.3 region covered by the DNA FISH probe (Figures 6D and S6F).

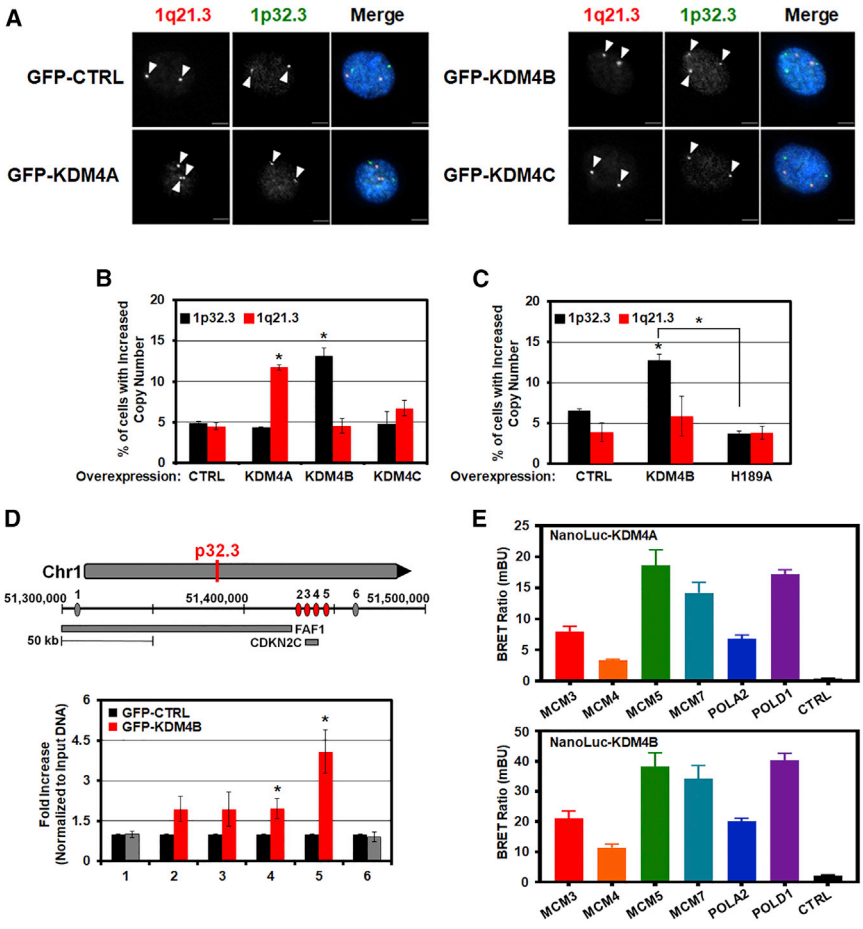

Figure 6. KDM4B Promotes Site-Specific Copy Gains and Rereplication at 1p32.3

(A) Representative images from DNA FISH of 1q21.3 (red), 1p32.3 (green), and DAPI (blue) merge after KDM4 family overexpression.

(B) DNA FISH after KDM4 overexpression.

(C) 1p32.3 copy gains are dependent upon KDM4B catalytic activity.

(D) Schematic depicting the location of the genomic primers used for rereplication. The location is based on genome assembly GRCh37-hg19. The primers labeled as 1 through 6 encompass the regions covered by the 1p32.3 FISH probe. The fold change in rereplication compared to control DNA is shown.

(E) NanoBRET assays for KDM4A (top panel) and KDM4B (bottom panel) are shown.

Error bars represent the SEM. *$p < 0.05$ by two-tailed Student's t test. Scale bar, 5 μm.

Consistent with KDM4B overexpression causing rereplication and copy gains, mass spectrometry analyses identified an association of KDM4B with replication machinery proteins (i.e., MCM3, MCM5, MCM7, RFC3, and DNAJA3) that was verified by co-immunoprecipitation analyses (Figures S6G and S6H and Table S4). These interactions were also confirmed *in vivo* by using NanoBRET (short for nano-luciferase bioluminescent resonance energy transfer), a proximity based protein:protein interaction live-cell assay. Consistent with our previous discovery (Black et al., 2013), KDM4A interacted with the MCM proteins and DNA polymerases (Figure 6E, top panel). In addition, energy transfer between KDM4B and the MCMs and DNA polymerase subunits were observed to varying degrees across multiple subunits within these larger complexes, which indicates association of KDM4B with these protein complexes (Figure 6E, bottom panel and Figure S6I). Taken together, these results suggest that KDM4B directly associates with replication machinery to promote rereplication and copy gain of the 1p32.3 region.

Since KMT2A promoted 1p32.3 DNA copy gain in a KDM4A-independent manner (Figure 4G), we tested whether KDM4B was required for KMT2A-generated copy gains of 1p32.3. KDM4B depletion abrogated KMT2A-generated 1p32.3 copy gains, demonstrating that KDM4B was essential for the copy gain generation by KMT2A (Figures 7A, S7A, and S7B). KDM4B was also required for the copy gain generated with KDM5B depletion, while KDM4A depletion did not have any effect on 1p32.3 copy gains (Figures 7B and S7C–S7G). Consistent with this observation, 1p32.3 generated with KDM5i treatment was also blocked with KDM4B depletion (Figures 7C and S7H). Furthermore, the introduction of the H3K4M mutant abrogated the 1p32.3 copy gain generated by KDM4B overexpression (Figures 7D, S3F, S7I, and S7J), which suggests that KDM4B recruitment on chromatin occurs via H3K4 methylation. Consistent with this possibility, the NanoBRET assay demonstrated that cells expressing H3K4M had reduced KDM4B associated with chromatin *in vivo* (Figures 7E and 7F).

Our data suggest that KDM4B recruitment is required for the rereplication and 1p32.3 copy gains. By ChIP, KDM4B enrichment was observed at the rereplication sites upon stable overexpression (Figure 7G). Furthermore, siRNA depletion of KDM4B in KDM4B-overexpressing cells reduced the occupancy of KDM4B to the baseline level at the rereplicated regions (1p32.3-4 and 1p32.3-5, Figures S7K and S7L). Since KDM4B catalyzes demethylation of histone lysine 9 and lysine 36 residues, we tested whether direct methylation interference by introducing H3K9M and H3K36M histone mutations would induce 1p32.3 copy gains (Black et al., 2013). Introduction of both K9M and K36M caused copy gains of the 1q12h, 1q21.2, and 1q21.3 regions (Figures 7H and S7M–S7Q), which was consistent with our previous report (Black et al., 2013, 2015). However, only H3K36M caused the 1p32.3 locus to undergo copy gains, while a non-copy-gained region 1q23.3 remained unchanged (Figures 7H and S7Q), suggesting specificity for H3K36 methylation in causing 1p32.3 copy gains.

Since KDM4B is recruited to the rereplicated and copy-gained region and the copy gains are catalytically dependent, we assessed the impact of KDM4B overexpression on H3K36me3

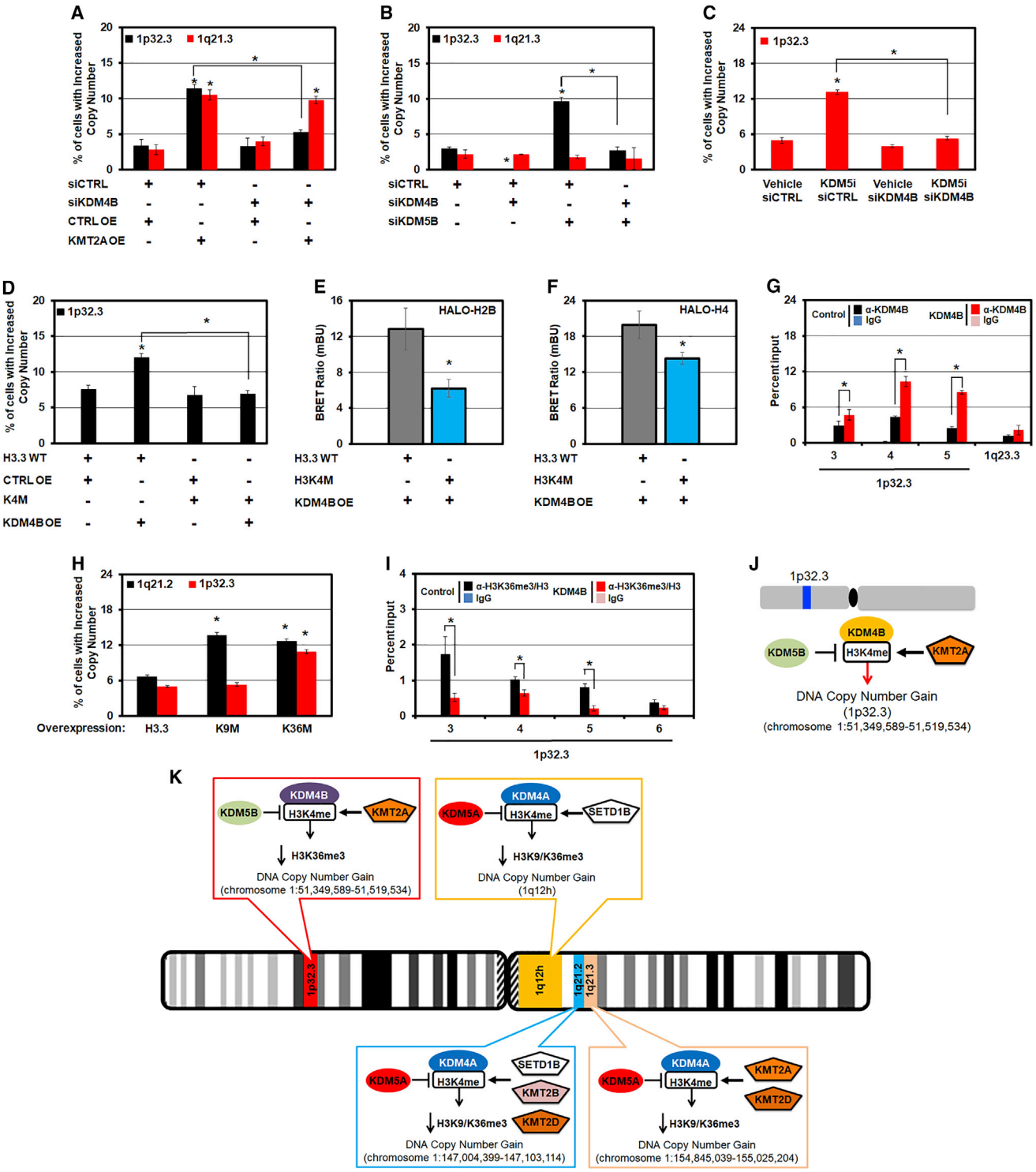

Figure 7. 1p32.3 TSSG Formation Correlated with KDM4B Recruitment and Reduced H3K36me3

(A) After KDM4B depletion and KMT2A overexpression, DNA FISH was conducted.

(B) KDM4B knockdown blocks siKDM5B associated 1p32.3 copy gains.

(C) KDM4B depletion rescued KDM5i mediated 1p32.3 copy gains.

(D) H3K4M transduction blocked 1p32.3 copy gains generated by KDM4B overexpression.

(E and F) Graph of RPE cells transduced with either wild-type H3 or H3K4M before being transiently transfected with NanoLuc-KDM4B (KDM4B OE) along with HALO-H2B (E) or HALO-H4 (F).

(legend continued on next page)

at 1p32.3 locus. A significant decrease in the H3K36me3 levels occurred with KDM4B overexpression at the rereplicated region (i.e., 1p32.3-3, −4 and −5), while a non-rereplicated region (1p32.3-6) remained unaffected (Figures 7I and S7R). Taken together, these data suggest that KDM4B recruitment and catalytic activity is essential for reducing H3K36me3 at the rereplicated and copy-gained 1p32.3 locus (Figure 7J). These results highlight the importance of localized chromatin states and appropriate KMT-KDM balance in preserving DNA copy number within the genome (Figure 7K).

DISCUSSION

We have identified a compendium of epigenetic factors, specifically lysine methyltransferases and demethylases, that directly impact locus-specific DNA copy gains (Figure 7K). These chromatin modulators control histone lysine 4 methylation state and, in turn, coordinate specific H3K9 and K36 tri-demethylases to regulate rereplication and DNA copy gains of specific genomic loci. Our results uncover a mechanism for achieving site-specific copy gains through the cross-talk of eight chromatin regulators and their modulation of localized chromatin states. These studies have broad implications in understanding how genomes undergo amplification during development, stress conditions, and disease states.

H3K4 Methylation and TSSGs

Chromatin and chromosomal architecture play an important role in DNA replication and, in turn, genome stability (Dileep et al., 2015; MacAlpine and Almouzni, 2013; Smith and Aladjem, 2014). For example, H3K4 methylation has been suggested to promote rereplication (Huang et al., 2016; Lu et al., 2016b). Specifically, WDR5 depletion, which blocks most COMPASS family of H3K4 KMTs, reduced the rereplication and the polyploidy phenotype observed when replication licensing was disrupted (Lu et al., 2016b). Consistent with this observation, histone lysine 4 demethylases regulate DNA replication. For instance, KDM5C/JARID1C regulated the pre-initiation complex assembly and proper firing of the early replication origins (Rondinelli et al., 2015), while KDM5A regulated ORC recruitment to origin sites and thus proper regulation of replication (Huang et al., 2016).

Our results suggest that COMPASS H3K4 KMT enzymes and the H3K4 tri-demethylases are controlling rereplication and DNA copy gains at specific loci. The balance between H3K4 KMTs and KDMs "toggle" H3K4 methylation at specific loci, which then regulates their ability to rereplicate and copy gain. Consistent with this hypothesis, each KDM5 H3K4 tri-demethylase controls a distinct subset of TSSG sites. Specifically, KDM5A controlled 1q12h, 1q21.2, and 1q21.3, while KDM5B regulated 1p32.3 (Figure 7K). In fact, KDM5i allowed all the observed TSSGs to emerge. Similarly, each COMPASS-family H3K4 methyltransferase regulated distinct genomic sites within the subset of known TSSGs being generated (Figure 7K). However, interference with H3K4 methylation by introducing H3K4M was able to suppress all the observed TSSGs. The H3K4M and KDM5i experiments emphasize that H3K4 methylation is a critical determinant of rereplication and that there is an exquisite specificity in KMTs-KDMs in controlling site-specific amplifications. These data suggest an epigenetic addressing system for controlling site-specific amplifications and underscore the importance of regulating the local chromatin states so that DNA amplifications are prevented or allowed to occur.

KMT-KDM Cross-Talk Generates TSSGs

KDM4A-dependent TSSGs required the Tudor domains (Black et al., 2013). These domains recognized H4K20me2/3 and H3K4me3 (Huang et al., 2006; Mallette et al., 2012; Spektor and Rice, 2009). However, the significance of either set of modifications in modulating KDM4A-driven biology remained an unanswered question. In this study, H3K4 methylation was critical for the KDM4A-dependent regulation of site-specific rereplication and DNA copy gains. For example, KDM5A depletion resulted in rereplication and TSSG formation for specific genomic loci that were dependent on increased H3K4 methylation and KDM4A recruitment. Furthermore, SETD1B, KMT2A, KMT2B, and KMT2D modulated subsets of loci that undergo copy gains upon KDM5A depletion and KDM4A overexpression. Therefore, we propose that increased H3K4me3 helps hone KDM4A recruitment through its Tudor domain and promotes more permissive chromatin for DNA rereplication.

We have also identified a non-KDM4A-dependent copy number regulation of chromosome 1p32.3 locus by a network of KDM5B-KDM4B-KMT2A histone modifying proteins. KDM4B also required H3K4 methylation to generate the 1p32.3 TSSG. KMT2A was necessary for KDM4B copy gains, while KDM5B prevented them. Furthermore, disruption of H3K4 methylation caused less KDM4B on the chromatin, illustrating the importance of this modification in recruiting another KDM4 member and, in turn, site-specific rereplication and DNA amplification. Our results suggest the existence of a complex molecular network of KMTs and KDMs that regulate site-specific copy gains and emphasize the importance of the KDM4 members in generating TSSGs. Therefore, chemical (Black et al., 2015) or RNA-based strategies (Black et al., 2016) targeting the KDM4 family could have a profound effect on DNA copy number heterogeneity in diseases such as cancer. Future studies need to identify other genomic and epigenomic features that are important for targeting the KMTs and KDMs to their associated TSSGs. Additional features (e.g., insulator elements, enhancers, CpG islands, and other DNA and histone modifications) likely function in concert with H3K4me3 to facilitate the recruitment of KMTs and KDMs to maintain DNA copy number control. Since

(G) KDM4B ChIP from control and GFP-KDM4B stably overexpressing cells. The positions are noted in Figure 6D.
(H) DNA FISH in cells transduced with H3.3K9M and -K36M.
(I) A graph containing the H3K36me3/H3 ratio for control and GFP-KDM4B cells at the indicated genomic regions (see Figure 6D).
(J) A model depicting the interplay among KDM5B-KDM4B-KMT2A at 1p32.3 is shown.
(K) A model summarizing the KMT-KDM cross-talk at multiple chromosome 1 loci. The locations are based on genome assembly GRCh37-hg19. Error bars represent the SEM. *$p < 0.05$ by two-tailed Student's t test.

H3K4 methylation was required for the TSSGs, active transcription or select RNAs could also be important in TSSG formation. For example, the mis-expression of the HSATII repeat RNA promoted expansions in pericentromeric regions (Bersani et al., 2015). Furthermore, extrachromosomal circular DNA elements were observed in gene-rich chromosomal regions (Møller et al., 2018), which suggests a relationship between extrachromosomal generation and actively marked regions. Therefore, the relationship between RNA mis-expression and TSSG formation needs further evaluation.

Our studies illustrate the importance of systematically targeting the KDM families in order to either promote or block DNA copy gains (Figures 3, 4, and 7). The ability to therapeutically control DNA amplifications could have profound implications in the areas of tumor heterogeneity and drug responses. Consistent with this possibility, KDM5 inhibition resulted in TSSGs and a reduced response to low dose cisplatin exposure across multiple cancer cell types (Figures S7S–S7Y). Future studies need to explore these preliminary observations and establish the role of specific TSSGs in drug responses. For example, does the reduced drug response that parallels DNA copy gains result from the general mechanism of TSSG formation (e.g., increasing the baseline of DNA copies) and/or result from the increased copies and expression of the associated drug-resistant oncogenes (e.g., *CKS1B* within 1q21.3)?

KDM4A amplified TSSGs were generated in the presence of both H3K9M and H3K36M; however, the KDM4B-copy-gained locus was specific to H3K36M. It is possible that the amplifications of specific regions are distinctly controlled by K36 and/or K9 methylation states. H3K36M is a known "onco-histone" associated with certain tumor types (Fang et al., 2016; Kallappagoudar et al., 2015; Lu et al., 2016a; Papillon-Cavanagh et al., 2017; Behjati et al., 2013). Delineating how this onco-histone contributes to the tumor pathogenesis, especially from the perspective of maintaining replication fidelity and genome integrity, would be of paramount importance. Identifying the epigenetic landscape that underlies the onco-histone associated amplifications from our study in the relevant tumor models can shed light into the biology and tumorigenic mechanisms.

Future studies should also interrogate how mutations and genomic alterations within the KMT-KDM network can modulate DNA amplifications in the genome. For example, do known mutations or rearrangements in COMPASS family members alter the composition of DNA amplifications in the human genome (Lawrence et al., 2014; Lawrence et al., 2013; Van Rechem and Whetstine, 2014)? Furthermore, we hypothesize that cellular cues and exposures could have an impact on mechanisms generating TSSGs. The extracellular environment and metabolic exposures have been implicated in promoting tumor heterogeneity (Almendro et al., 2013; Burrell et al., 2013; Meacham and Morrison, 2013). A recent study demonstrated that signaling network analyses provided associations with DNA amplifications (Graham et al., 2017). Consistent with this hypothesis, hypoxia generated TSSGs through KDM4A stabilization, which was blocked when cells were exposed to succinate, a natural metabolite that inhibits KDMs (Black et al., 2015; Smith et al., 2007). Therefore, future studies should explore the impact that genetic variants and cellular exposures have on TSSG formation so that mechanisms promoting DNA copy amplifications can be resolved.

KDM5-Related TSSG Kinetics

KDM5A depletion resulted in TSSGs that occur outside of S phase, which was consistent with a previous report suggesting that replication occurred inappropriately (Huang et al., 2016). However, the appearance of these TSSGs is in sharp contrast to KDM4A overexpression alone (Black et al., 2013). These data suggest that the H3K4 methylation state provides a permissive chromatin environment that allows recruitment and rereplication outside of S phase. KDM5A depletion would allow this modification to persist and promote KDM4A driven copy gains, whereas resetting the H3K4 methylation would block KDM4A recruitment upon KDM5A overexpression. Consistent with this model, KDM4A was recruited to enriched H3K4me3 sites at rereplicated regions. DNA polymerase alpha was enriched at copy-gained sites and EdU positive cells were increased in late G2 upon KDM5A depletion. Furthermore, H3K4M blocked the TSSGs generated by KDM4A overexpression and KDM5A depletion. These data highlight the importance of the localized chromatin environment in controlling site-specific rereplication and copy gains. However, we cannot rule out the possibility that KDM5A depletion also impacts an unknown mechanism(s) promoting copy gain removal.

Our study documents a repertoire of chromatin regulators that can generate transient DNA copy gains (Figure 7K). Given different cellular division rates within tissues and tumors, the differentially cycling cells could create significant heterogeneity as a consequence of rereplicated fragment generation. The expression, activity, and mutational status of the identified KMTs and KDMs could impact the spatial and temporal regulation of the rereplicated fragments. Therefore, cells that are actively dividing and have the appropriate genetic background will be able to execute these alterations, which could provide a basis for DNA copy number heterogeneity within a tissue and/or tumor (Mishra and Whetstine, 2016). Whether these fragments can be integrated and persist after G2 phase remain to be discovered. Nonetheless, these transiently generated copy gains could be generated in each cycle and then resolved by yet-undiscovered mechanisms. Future studies need to elucidate the pathways regulating the removal and regulation of TSSGs and whether these pathways work together with epigenetic dysregulation to control tumor heterogeneity and drug responses, which will ultimately identify novel diagnostic and therapeutic options.

STAR★METHODS

Detailed methods are provided in the online version of this paper and include the following:

- KEY RESOURCES TABLE
- CONTACT FOR REAGENT AND RESOURCE SHARING
- EXPERIMENTAL MODEL AND SUBJECT DETAILS
  - Cell Culture
- METHOD DETAILS

SUPPLEMENTAL INFORMATION

Supplemental Information includes seven figures and five tables and can be found with this article online at https://doi.org/10.1016/j.cell.2018.06.018.

A video abstract is available at https://doi.org/10.1016/j.cell.2018.06.018#mmc6.

ACKNOWLEDGMENTS

We are grateful to Ravi Mylvaganam, Christina Luo, and the MGH Flow Cytometry Core for assistance with flow cytometry. We thank Ali Shilatifard (Northwestern University) for providing the MDA-MB-231 SET1B (SETD1B) SET domain deleted cells. We also thank Peter Lewis (University of Wisconsin) for the H3K-M constructs. We thank Brittany Sexton, Megan Dillingham, Paul Burrowes, and Daniel Ananth for technical contributions. We would like to thank Miguel Rivera, Mark Cobbold, Kurt Isselbacher, Mo Motamedi, and Deepak Jha for comments on the manuscript. Work related to this study is supported by the American Cancer Society (J.R.W.; RSG-13-115-01-CCG) and R01GM097360 (J.R.W.). J.R.W. is a Tepper Family Massachusetts General Hospital Scholar and Leukemia and Lymphoma Scholar, as well as a recipient of an American Lung Association Lung Cancer Discovery Award and an Innovation Award from the Alex Lemonade Stand Foundation. S.M. was supported by a Senior Research Training Fellowship from the American Lung Association. T.L.C. is supported by an EMBO long term fellowship (EMBO ALTF 449-2017), and D.C. is a recipient of Ovarian Cancer Research Fund Alliance (Ann and Sol Schreiber Mentored Investigator Award-543667).

AUTHOR CONTRIBUTIONS

J.R.W. conceived the study and associated concepts. J.R.W. and S.M. conceptualized and designed the experiments, and S.M. conducted and analyzed the majority of the experiments. C.V.R., S.P., T.L.C., D.C., S.D.M., J.C.B., S.E.M., M.S.L., and D.L.D. contributed to and/or conducted experiments and their interpretation within the manuscript. J.R.W. and S.M. wrote the paper with input and assistance from other authors.

DECLARATION OF INTERESTS

D.L.D. and S.D.M. are employees of Promega. Promega holds the patent on Halo Tag and NanoLuc. J.R.W. receives research support from Astrazeneca. J.R.W. consults for Qsonica. J.R.W. is a named inventor on an unpublished patent application related to this work.

Received: November 2, 2017
Revised: April 2, 2018
Accepted: June 8, 2018
Published: July 26, 2018; corrected online: November 12, 2018

REFERENCES

Almendro, V., Marusyk, A., and Polyak, K. (2013). Cellular heterogeneity and molecular evolution in cancer. Annu. Rev. Pathol. *8*, 277–302.

Alt, F.W., Kellems, R.E., Bertino, J.R., and Schimke, R.T. (1978). Selective multiplication of dihydrofolate reductase genes in methotrexate-resistant variants of cultured murine cells. J. Biol. Chem. *253*, 1357–1370.

Behjati, S., Tarpey, P.S., Presneau, N., Scheipl, S., Pillay, N., Van Loo, P., Wedge, D.C., Cooke, S.L., Gundem, G., Davies, H., et al. (2013). Distinct H3F3A and H3F3B driver mutations define chondroblastoma and giant cell tumor of bone. Nat. Genet. *45*, 1479–1482.

Beroukhim, R., Mermel, C.H., Porter, D., Wei, G., Raychaudhuri, S., Donovan, J., Barretina, J., Boehm, J.S., Dobson, J., Urashima, M., et al. (2010). The landscape of somatic copy-number alteration across human cancers. Nature *463*, 899–905.

Bersani, F., Lee, E., Kharchenko, P.V., Xu, A.W., Liu, M., Xega, K., MacKenzie, O.C., Brannigan, B.W., Wittner, B.S., Jung, H., et al. (2015). Pericentromeric satellite repeat expansions through RNA-derived DNA intermediates in cancer. Proc. Natl. Acad. Sci. USA *112*, 15148–15153.

Biedler, J.L., and Spengler, B.A. (1976a). Metaphase chromosome anomaly: association with drug resistance and cell-specific products. Science *191*, 185–187.

Biedler, J.L., and Spengler, B.A. (1976b). A novel chromosome abnormality in human neuroblastoma and antifolate-resistant Chinese hamster cell lives in culture. J. Natl. Cancer Inst. *57*, 683–695.

Black, J.C., Allen, A., Van Rechem, C., Forbes, E., Longworth, M., Tschöp, K., Rinehart, C., Quiton, J., Walsh, R., Smallwood, A., et al. (2010). Conserved antagonism between JMJD2A/KDM4A and HP1γ during cell cycle progression. Mol. Cell *40*, 736–748.

Black, J.C., Manning, A.L., Van Rechem, C., Kim, J., Ladd, B., Cho, J., Pineda, C.M., Murphy, N., Daniels, D.L., Montagna, C., et al. (2013). KDM4A lysine demethylase induces site-specific copy gain and rereplication of regions amplified in tumors. Cell *154*, 541–555.

Black, J.C., Atabakhsh, E., Kim, J., Biette, K.M., Van Rechem, C., Ladd, B., Burrowes, P.D., Donado, C., Mattoo, H., Kleinstiver, B.P., et al. (2015). Hypoxia drives transient site-specific copy gain and drug-resistant gene expression. Genes Dev. *29*, 1018–1031.

Black, J.C., Zhang, H., Kim, J., Getz, G., and Whetstine, J.R. (2016). Regulation of Transient Site-specific Copy Gain by MicroRNA. J. Biol. Chem. *291*, 4862–4871.

Burrell, R.A., McGranahan, N., Bartek, J., and Swanton, C. (2013). The causes and consequences of genetic heterogeneity in cancer evolution. Nature *501*, 338–345.

Christensen, J., Agger, K., Cloos, P.A., Pasini, D., Rose, S., Sennels, L., Rappsilber, J., Hansen, K.H., Salcini, A.E., and Helin, K. (2007). RBP2 belongs to a family of demethylases, specific for tri-and dimethylated lysine 4 on histone 3. Cell *128*, 1063–1076.

Dileep, V., Rivera-Mulia, J.C., Sima, J., and Gilbert, D.M. (2015). Large-Scale Chromatin Structure-Function Relationships during the Cell Cycle and Development: Insights from Replication Timing. Cold Spring Harb Symp Quant Biol. *2015*, 53–63.

Diskin, S.J., Hou, C., Glessner, J.T., Attiyeh, E.F., Laudenslager, M., Bosse, K., Cole, K., Mossé, Y.P., Wood, A., Lynch, J.E., et al. (2009). Copy number variation at 1q21.1 associated with neuroblastoma. Nature *459*, 987–991.

Fang, D., Gan, H., Lee, J.H., Han, J., Wang, Z., Riester, S.M., Jin, L., Chen, J., Zhou, H., Wang, J., et al. (2016). The histone H3.3K36M mutation reprograms the epigenome of chondroblastomas. Science *352*, 1344–1348.

Fonseca, R., Van Wier, S.A., Chng, W.J., Ketterling, R., Lacy, M.Q., Dispenzieri, A., Bergsagel, P.L., Rajkumar, S.V., Greipp, P.R., Litzow, M.R., et al. (2006). Prognostic value of chromosome 1q21 gain by fluorescent in situ hybridization and increase CKS1B expression in myeloma. Leukemia *20*, 2034–2040.

Graham, N.A., Minasyan, A., Lomova, A., Cass, A., Balanis, N.G., Friedman, M., Chan, S., Zhao, S., Delgado, A., Go, J., et al. (2017). Recurrent patterns of DNA copy number alterations in tumors reflect metabolic selection pressures. Mol. Syst. Biol. *13*, 914.

Haber, D.A., and Schimke, R.T. (1981). Unstable amplification of an altered dihydrofolate reductase gene associated with double-minute chromosomes. Cell *26*, 355–362.

Hoshii, T., Cifani, P., Feng, Z., Huang, C.H., Koche, R., Chen, C.W., Delaney, C.D., Lowe, S.W., Kentsis, A., and Armstrong, S.A. (2018). A Non-catalytic Function of SETD1A Regulates Cyclin K and the DNA Damage Response. Cell *172*, 1007–1021.

Hu, D., Gao, X., Morgan, M.A., Herz, H.M., Smith, E.R., and Shilatifard, A. (2013). The MLL3/MLL4 branches of the COMPASS family function as major histone H3K4 monomethylases at enhancers. Mol. Cell. Biol. *33*, 4745–4754.

Hu, D., Gao, X., Cao, K., Morgan, M.A., Mas, G., Smith, E.R., Volk, A.G., Bartom, E.T., Crispino, J.D., Di Croce, L., et al. (2017). Not All H3K4 Methylations Are Created Equal: Mll2/COMPASS Dependency in Primordial Germ Cell Specification. Mol Cell *65*, 460–475.

Huang, Y., Fang, J., Bedford, M.T., Zhang, Y., and Xu, R.M. (2006). Recognition of histone H3 lysine-4 methylation by the double tudor domain of JMJD2A. Science *312*, 748–751.

Huang, C., Cheng, J., Bawa-Khalfe, T., Yao, X., Chin, Y.E., and Yeh, E.T.H. (2016). SUMOylated ORC2 Recruits a Histone Demethylase to Regulate Centromeric Histone Modification and Genomic Stability. Cell Rep. *15*, 147–157.

Inoue, J., Otsuki, T., Hirasawa, A., Imoto, I., Matsuo, Y., Shimizu, S., Taniwaki, M., and Inazawa, J. (2004). Overexpression of PDZK1 within the 1q12-q22 amplicon is likely to be associated with drug-resistance phenotype in multiple myeloma. Am. J. Pathol. *165*, 71–81.

Iwase, S., Lan, F., Bayliss, P., de la Torre-Ubieta, L., Huarte, M., Qi, H.H., Whetstine, J.R., Bonni, A., Roberts, T.M., and Shi, Y. (2007). The X-linked mental retardation gene SMCX/JARID1C defines a family of histone H3 lysine 4 demethylases. Cell *128*, 1077–1088.

Jiang, X.R., Jimenez, G., Chang, E., Frolkis, M., Kusler, B., Sage, M., Beeche, M., Bodnar, A.G., Wahl, G.M., Tlsty, T.D., and Chiu, C.P. (1999). Telomerase expression in human somatic cells does not induce changes associated with a transformed phenotype. Nat. Genet. *21*, 111–114.

Johansson, C., Velupillai, S., Tumber, A., Szykowska, A., Hookway, E.S., Nowak, R.P., Strain-Damerell, C., Gileadi, C., Philpott, M., Burgess-Brown, N., et al. (2016). Structural analysis of human KDM5B guides histone demethylase inhibitor development. Nat. Chem. Biol. *12*, 539–545.

Kallappagoudar, S., Yadav, R.K., Lowe, B.R., and Partridge, J.F. (2015). Histone H3 mutations–a special role for H3.3 in tumorigenesis? Chromosoma *124*, 177–189.

Kim, T.M., Xi, R., Luquette, L.J., Park, R.W., Johnson, M.D., and Park, P.J. (2013). Functional genomic analysis of chromosomal aberrations in a compendium of 8000 cancer genomes. Genome Res. *23*, 217–227.

Klose, R.J., Yan, Q., Tothova, Z., Yamane, K., Erdjument-Bromage, H., Tempst, P., Gilliland, D.G., Zhang, Y., and Kaelin, W.G., Jr. (2007). The retinoblastoma binding protein RBP2 is an H3K4 demethylase. Cell *128*, 889–900.

Kudoh, K., Takano, M., Koshikawa, T., Hirai, M., Yoshida, S., Mano, Y., Yamamoto, K., Ishii, K., Kita, T., Kikuchi, Y., et al. (1999). Gains of 1q21-q22 and 13q12-q14 are potential indicators for resistance to cisplatin-based chemotherapy in ovarian cancer patients. Clin. Cancer Res. *5*, 2526–2531.

Lawrence, M.S., Stojanov, P., Polak, P., Kryukov, G.V., Cibulskis, K., Sivachenko, A., Carter, S.L., Stewart, C., Mermel, C.H., Roberts, S.A., et al. (2013). Mutational heterogeneity in cancer and the search for new cancer-associated genes. Nature *499*, 214–218.

Lawrence, M.S., Stojanov, P., Mermel, C.H., Robinson, J.T., Garraway, L.A., Golub, T.R., Meyerson, M., Gabriel, S.B., Lander, E.S., and Getz, G. (2014). Discovery and saturation analysis of cancer genes across 21 tumour types. Nature *505*, 495–501.

Lee, J.E., Wang, C., Xu, S., Cho, Y.W., Wang, L., Feng, X., Baldridge, A., Sartorelli, V., Zhuang, L., Peng, W., and Ge, K. (2013). H3K4 mono- and di-methyltransferase MLL4 is required for enhancer activation during cell differentiation. eLife *2*, e01503.

Lu, C., Jain, S.U., Hoelper, D., Bechet, D., Molden, R.C., Ran, L., Murphy, D., Venneti, S., Hameed, M., Pawel, B.R., et al. (2016a). Histone H3K36 mutations promote sarcomagenesis through altered histone methylation landscape. Science *352*, 844–849.

Lu, F., Wu, X., Yin, F., Chia-Fang Lee, C., Yu, M., Mihaylov, I.S., Yu, J., Sun, H., and Zhang, H. (2016b). Regulation of DNA replication and chromosomal polyploidy by the MLL-WDR5-RBBP5 methyltransferases. Biol. Open *5*, 1449–1460.

MacAlpine, D.M., and Almouzni, G. (2013). Chromatin and DNA replication. Cold Spring Harb. Perspect. Biol. *5*, a010207.

Mallette, F.A., Mattiroli, F., Cui, G., Young, L.C., Hendzel, M.J., Mer, G., Sixma, T.K., and Richard, S. (2012). RNF8- and RNF168-dependent degradation of KDM4A/JMJD2A triggers 53BP1 recruitment to DNA damage sites. EMBO J. *31*, 1865–1878.

Meacham, C.E., and Morrison, S.J. (2013). Tumour heterogeneity and cancer cell plasticity. Nature *501*, 328–337.

Mishra, S., and Whetstine, J.R. (2016). Different Facets of Copy Number Changes: Permanent, Transient, and Adaptive. Mol. Cell. Biol. *36*, 1050–1063.

Møller, H.D., Mohiyuddin, M., Prada-Luengo, I., Sailani, M.R., Halling, J.F., Plomgaard, P., Maretty, L., Hansen, A.J., Snyder, M.P., Pilegaard, H., et al. (2018). Circular DNA elements of chromosomal origin are common in healthy human somatic tissue. Nat. Commun. *9*, 1069.

Nathanson, D.A., Gini, B., Mottahedeh, J., Visnyei, K., Koga, T., Gomez, G., Eskin, A., Hwang, K., Wang, J., Masui, K., et al. (2014). Targeted therapy resistance mediated by dynamic regulation of extrachromosomal mutant EGFR DNA. Science *343*, 72–76.

Papillon-Cavanagh, S., Lu, C., Gayden, T., Mikael, L.G., Bechet, D., Karamboulas, C., Ailles, L., Karamchandani, J., Marchione, D.M., Garcia, B.A., et al. (2017). Impaired H3K36 methylation defines a subset of head and neck squamous cell carcinomas. Nat. Genet. *49*, 180–185.

Pedersen, M.T., Kooistra, S.M., Radzisheuskaya, A., Laugesen, A., Johansen, J.V., Hayward, D.G., Nilsson, J., Agger, K., and Helin, K. (2016). Continual removal of H3K9 promoter methylation by Jmjd2 demethylases is vital for ESC self-renewal and early development. EMBO J. *35*, 1550–1564.

Petersen, S., Aninat-Meyer, M., Schlüns, K., Gellert, K., Dietel, M., and Petersen, I. (2000). Chromosomal alterations in the clonal evolution to the metastatic stage of squamous cell carcinomas of the lung. Br. J. Cancer *82*, 65–73.

Rondinelli, B., Schwerer, H., Antonini, E., Gaviraghi, M., Lupi, A., Frenquelli, M., Cittaro, D., Segalla, S., Lemaitre, J.M., and Tonon, G. (2015). H3K4me3 demethylation by the histone demethylase KDM5C/JARID1C promotes DNA replication origin firing. Nucleic Acids Res. *43*, 2560–2574.

Shilatifard, A. (2012). The COMPASS family of histone H3K4 methylases: mechanisms of regulation in development and disease pathogenesis. Annu. Rev. Biochem. *81*, 65–95.

Smith, O.K., and Aladjem, M.I. (2014). Chromatin structure and replication origins: determinants of chromosome replication and nuclear organization. J. Mol. Biol. *426*, 3330–3341.

Smith, E.H., Janknecht, R., and Maher, L.J., 3rd. (2007). Succinate inhibition of alpha-ketoglutarate-dependent enzymes in a yeast model of paraganglioma. Hum. Mol. Genet. *16*, 3136–3148.

Spektor, T.M., and Rice, J.C. (2009). Identification and characterization of posttranslational modification-specific binding proteins in vivo by mammalian tethered catalysis. Proc. Natl. Acad. Sci. USA *106*, 14808–14813.

Su, Z., Wang, F., Lee, J.H., Stephens, K.E., Papazyan, R., Voronina, E., Krautkramer, K.A., Raman, A., Thorpe, J.J., Boersma, M.D., et al. (2016). Reader

domain specificity and lysine demethylase-4 family function. Nat. Commun. *7*, 13387.

Tajima, K., Yae, T., Javaid, S., Tam, O., Comaills, V., Morris, R., Wittner, B.S., Liu, M., Engstrom, A., Takahashi, F., et al. (2015). SETD1A modulates cell cycle progression through a miRNA network that regulates p53 target genes. Nat. Commun. *6*, 8257.

Turner, K.M., Deshpande, V., Beyter, D., Koga, T., Rusert, J., Lee, C., Li, B., Arden, K., Ren, B., Nathanson, D.A., et al. (2017). Extrachromosomal oncogene amplification drives tumour evolution and genetic heterogeneity. Nature *543*, 122–125.

Van Rechem, C., and Whetstine, J.R. (2014). Examining the impact of gene variants on histone lysine methylation. Biochim. Biophys. Acta *1839*, 1463–1476.

Van Rechem, C., Black, J.C., Abbas, T., Allen, A., Rinehart, C.A., Yuan, G.C., Dutta, A., and Whetstine, J.R. (2011). The SKP1-Cul1-F-box and leucine-rich repeat protein 4 (SCF-FbxL4) ubiquitin ligase regulates lysine demethylase 4A (KDM4A)/Jumonji domain-containing 2A (JMJD2A) protein. J. Biol. Chem. *286*, 30462–30470.

Van Rechem, C., Black, J.C., Boukhali, M., Aryee, M.J., Gräslund, S., Haas, W., Benes, C.H., and Whetstine, J.R. (2015). Lysine demethylase KDM4A associates with translation machinery and regulates protein synthesis. Cancer Discov. *5*, 255–263.

Wang, L., Collings, C.K., Zhao, Z., Cozzolino, K.A., Ma, Q., Liang, K., Marshall, S.A., Sze, C.C., Hashizume, R., Savas, J.N., and Shilatifard, A. (2017). A cytoplasmic COMPASS is necessary for cell survival and triple-negative breast cancer pathogenesis by regulating metabolism. Genes Dev. *31*, 2056–2066.

Zack, T.I., Schumacher, S.E., Carter, S.L., Cherniack, A.D., Saksena, G., Tabak, B., Lawrence, M.S., Zhsng, C.Z., Wala, J., Mermel, C.H., et al. (2013). Pan-cancer patterns of somatic copy number alteration. Nat. Genet. *45*, 1134–1140.

STAR★METHODS

KEY RESOURCES TABLE

REAGENT OR RESOURCE	SOURCE	IDENTIFIER
Antibodies		
anti-KDM4A, clone N154/21	UC Davis/ NIH NeuromAb	Cat# 75-189; RRID:AB_10671303
anti-KDM4A (used for ChIP)	Structural Genomic Consortium	Cat# P006
anti-KDM4A (used for ChIP)	Structural Genomic Consortium	Cat# P014
anti-KDM5A (used for western blot and ChIP)	Abcam	Cat# ab70892; RRID:AB_2280628
anti-KDM5A (used for ChIP)	Bethyl Laboratories	Cat# A300-897A
anti-KDM4B (used for ChIP and IP's)	Abcam	Cat# ab191434; RRID:AB_2721242
anti-KDM4B	Santacruz	Cat# sc-67192; RRID:AB_1125080
anti-MCM5	Abcam	Cat# ab6154; RRID:AB_305322
anti-MCM2	Abcam	Cat# ab6153; RRID:AB_305321
anti-H3	Abcam	Cat# ab1791; RRID:AB_302613
anti-H3K4me3	Millipore	Cat# 07-473; RRID:AB_1977252
anti-Polymerase alpha	Abcam	Cat# ab31777-100; RRID:AB_731976
anti-GFP	Neuro mAb	Cat# 73-131; RRID:AB_10671444
anti-FLAG	Sigma	Cat# A8592; RRID:AB_439702
anti-beta actin	Millipore	Cat# MAB1501; RRID:AB_2223041
anti-Actinin	Santacruz	Cat# sc-17829; RRID:AB_626633
Anti-H3K36me3	Abcam	Cat# ab9050; RRID:AB_306966
Goat anti-mouse HRP	Biorad	Cat# 170-6516; RRID:AB_11125547
Goat anti-rabbit HRP	GenScript	Cat# A00167
Chemicals, Peptides, and Recombinant Proteins		
Hydroxyurea	Sigma	Cat# H8627
RO-3306 CDK1/cyclin inhibitor	Enzo Life Sciences	Cat# ALX-270-463-M005
5-Bromo-2′-deoxyuridine	Sigma	Cat# B5002
Xcessbio KDM5-C70	Fisher Scientific	Cat# NC0732032
Propidium iodide solution	Sigma	Cat# P4864
Cisplatin	Abcam	Cat# Ab141398
Karyomax Colcemid	GIBCO	Cat# 15212-012
Proteinase K from Tritirachium album	Sigma	Cat# P6556
Ribonuclease A	Sigma	Cat# R4875
Formaldehyde	Electron Microscopy Sciences	Cat# 15686
DMEM/F12	Life Technologies	Cat# 11320033
Dulbecco's Modified Eagle's Medium - High Glucose	Sigma Aldrich	Cat# D5648
Roswell Park Memorial Institute Medium (RPMI) 1640	Sigma Aldrich	Cat# R6504
OPTI-MEM	Life Technologies	Cat# 31985070
Trypsin-0.25% EDTA	Life Technologies	Cat# 2520056
L-Glutamine	Life Technologies	Cat# 25030-081
Penicillin-Streptomycin	Life Technologies	Cat# 15140122
FBS	GIBCO	Cat# 26140-079
Lipofectamine 3000	Life Technologies	Cat# L3000015
FuGENE HD	Promega	Cat# E2311
HaloLink Resin	Promega	Cat# G6509

(*Continued on next page*)

Continued

REAGENT OR RESOURCE	SOURCE	IDENTIFIER
Critical Commercial Assays		
miRNeasy Mini Kit	QIAGEN	Cat# 217004
Superscript IV 1st Strnd Systm	Life Technologies	Cat# 18091050
Click-IT EdU flow cytometry kit	Life Technologies	Cat# C10419
Click-iT EdU Alexa Fluor 488 Imaging Kit	Life Technologies	Cat# C10337
Lumi-Light Western Blotting Substrate	Roche	Cat# 12015200001
SuperSignal West Pico Plus Chemiluminescent Substrate	Thermo Scientific	Cat# 34577
Pierce BCA Protein Assay	Thermo Scientific	Cat# 23223 and 23224
FISH Wash Buffer	Dako-Agilent	Cat# G9401A and G9402A
NanoBRET Nano-Glo Detection System	Promega	Cat# N1661
Experiment Models: Cell Lines		
RPE-hTERT1	Nick Dyson	N/A
293T	ATCC	CRL-1573
SK-N-AS	ATCC	CRL-2137
H2591	Cyril Benes	N/A
MDA-MB-231	ATCC	HTB-26
OVCAR5	Cyril Benes	N/A
MDA-MB-231 Wild type SETD1B	Ali Shilatifard	N/A
MDA-MB-231 SETD1B set delete clone 22	Ali Shilatifard	N/A
MDA-MB-231 SETD1B set delete clone 25	Ali Shilatifard	N/A
Oligonucleotides		
See Table S3 for all the primers used for qRT-PCRs.	This study	N/A
See Table S5 for all the siRNA sequences.	Life Technologies	N/A
KDM5A shRNA clone_ TRCN0000014629, CCAGAC TTACAGGGACACTTA	MPL Core Facility	N/A
KDM5A shRNA clone_ TRCN0000014632, CCTTGA AAGAAGCCTTACAAA	MPL Core Facility	N/A
KDM5B shRNA clone_ TRCN0000014762, CGAGAT GGAATTAACAGTCTT	MPL Core Facility	N/A
Recombinant DNA		
HALO-KMT2A (HALO-MLL1)	Promega	N/A
HALO-KMT2B (Gene ID: 9757)	Promega	N/A
HALO-KMT2D (Gene ID: 8085)	Promega	N/A
HALO-SETD1A	Promega	N/A
HALO-KDM5B	Promega	N/A
HALO-KDM5A	Promega	N/A
GFP-SETD1B	GeneCopoeia	Cat# GC-H3298-GS
GFP-KDM4A	This study	N/A
GFP-KDM4B	This study	N/A
GFP-KDM4C	This study	N/A
pCDH-H3.3-FLAG-HA-PURO	Peter Lewis	N/A
pCDH-H3.3-K4M-FLAG-HA-PURO	Peter Lewis	N/A
pCDH-H3.3-K9M-FLAG-HA-PURO	Peter Lewis	N/A
pCDH-H3.3-K36M-FLAG-HA-PURO	Peter Lewis	N/A
HaloTag-MCM3	Promega	Cat# P25205
HaloTag-MCM4	Promega	Cat# P33991
HaloTag-MCM5	Promega	Cat# P33992
HaloTag-MCM7	Promega	Cat# P33993

(*Continued on next page*)

Continued

REAGENT OR RESOURCE	SOURCE	IDENTIFIER
HaloTag-POLA2	Promega	Cat# Q14181
HaloTag-POLD1	Promega	Cat# P28340
NanoLuc-KDM4A	Promega	Cat# O75164
NanoLuc-KDM4B	Promega	Cat# O94953
HaloTag alone	Promega	Cat# G6591
psPAX2	Nick Dyson	N/A
VSVG	Nick Dyson	N/A
Chromosome 1 classical satellite	Rainbow Scientific	Cat# LPE001-A
Chromosome 8 alpha satellite	Rainbow Scientific	Cat# LPE008-A
CKS1B/CDKN2C Amplification/Deletion probe	Rainbow Scientific	Cat# LPH039-A
SureFISH 1q21.2 BCL9	Agilent	Cat# G101190R
SureFISH 1p32.3 CDKN2C 153kb	Agilent	Cat# G101227R
SureFISH 1q23.3 PBX1 DF 603kb RD	Agilent	Cat# G101106R
Chromosome X alpha satellite	Rainbow Scientific	Cat# LPE0XR
Xq13.1, BAC Clone	CHORI BacPac	Cat# RP11-177A4
Chromosome 1 q telomere	Rainbow Scientific	Cat# LPT01QG-A
Software and Algorithms		
Slidebook 5.0	3i-Intelligent Imaging Innovations	https://www.intelligent-imaging.com/slidebook
Slidebook 6.0	3i-Intelligent Imaging Innovations	https://www.intelligent-imaging.com/slidebook
Scaffold	Proteome Software	http://www.proteomesoftware.com/products/scaffold

CONTACT FOR REAGENT AND RESOURCE SHARING

Requests for reagents and resources may be directed to the Lead Contact, Johnathan R. Whetstine (jwhetstine@hms.harvard.edu).

EXPERIMENTAL MODEL AND SUBJECT DETAILS

Cell Culture

The generation of stable cells, plasmids, antibodies and chemicals used can be found in the key resource table. Retinal pigment epithelial (RPE) and 293T cells were cultured in DMEM-high glucose (Sigma) media with 10% fetal bovine serum (FBS), 100U/ml penicillin, 100ug/ml streptomycin, and 2mM L-glutamine. H2591 lung cancer cells were cultured in RPMI (Sigma) with 10% fetal bovine serum, 100U/ml penicillin, 100ug/ml streptomycin, and 2mM L-glutamine. SK-N-AS cells were maintained in DMEM/F12 (GIBCO) with 10% fetal bovine serum (FBS), 100U/ml penicillin, 100ug/ml streptomycin, and 2mM L-glutamine. OVCAR5 cells were maintained in RPMI 1640 (Sigma) with 10% fetal bovine serum (FBS), 100U/ml penicillin, 100ug/ml streptomycin, and 2mM L-glutamine, glucose (0.25 g/L) and 1mM sodium pyruvate. MDA-MB-231 were cultured in DMEM-high glucose (Sigma) media with 10% fetal bovine serum (FBS), 100U/ml penicillin, 100ug/ml streptomycin, and 2mM L-glutamine. RPE, 293T, OVCAR5, MDA-MB-231, and SK-N-AS cells are female cells. H2951 cells are male.

METHOD DETAILS

Plasmids, Constructs and BACs

The list of all the plasmids and constructs has been provided in the key resource table. The BAC clone, RP11-177A4, from CHORI BacPac was used to generate the FISH probes for Xq13.1. The information for this BAC is provided in key resource table and how the labeled probes were generated are in the DNA FISH section below.

Transfection Conditions

siRNA transfections were performed using Lipofectamine 3000 transfection reagent (Invitrogen) in the OPTI-MEM medium (Life Technologies). Transfections were changed to complete media after 4 hr of transfection, and cells were collected 72 hr post transfection. Transient overexpression transfections were performed using Lipofectamine 3000 transfection reagent and P3000 reagent (Life Technologies) in OPTI-MEM medium for 4 hr, followed by change to complete media. Silencer select negative controls and siRNAs were purchased from Life Technologies. Their sequences and catalog numbers are in Table S5. For co-transfection

experiments, both the siRNA's were co-transfected at the same time and collected at 72 hr from transfection (Figures 3C, Figures S4A–S4V). For siRNA/overexpression experiments, cells were transfected with siRNA's for 48 hr followed by 24 hr of plasmid overexpression (Figures 4B, 4D-E, 4G-H and 7A). For overexpression experiment in Figure 5F, cells were co-transfected with plasmids and collected 24 hr post expression. For Figures 7B and S7G, cells were first transfected with KDM4A/KDM4B siRNA's for 48 hr followed by another 48 hr of KDM5B siRNA transfections. At least two different siRNAs against every gene were used for every experiment. For overexpression studies, at least two independent plates were transfected.

shRNA Transfection or Transduction

The shRNA clones for KDM5A and KDM5B were provided by the MPL core facility (MGH). Virus was generated by co-transfection of shRNA plasmids along with the packaging plasmids (psPAX2 and VSVG) in 293T cells. The virus containing supernatant was collected after 24 hr. RPE cells were infected in the presence of 8 μg/ml polybrene for 12 hr with the virus containing supernatant. Two clones for KDM5A shRNA (TRCN0000014629 and TRCN0000014632) were transiently transfected to generate virus and the viral supernatant was infected in RPE cells and collected 72 hr post infection. We were not able to generate stable cell lines with these KDM5A shRNAs in RPE cells. Data presented are the averages from two independently infected KDM5A shRNA clones. One clone of KDM5B shRNA (TRCN0000014762) were stably generated and used in this study. The stable cells with pLKO shEGFP control and KDM5B shRNA were seeded and collected 72 hr later for analysis. Data presented are the averages from two independent experiments containing duplicates of KDM5B stable shRNAs in each experiment. At least two biological replicates from FISH experiments were counted double blinded.

Transduction with Histone H3.3 variants

Plasmids for H3.3 K4M, K9M and K36M mutants were provided by Peter Lewis (University of Wisconsin). Virus was generated by co-transfection of specific plasmids along with the packaging plasmids (AmphoPAK and VSVG) in 293T cells. The virus containing supernatant was collected after 24 hr. RPE cells were infected in the presence of 8 μg/ml polybrene for 12 hr with the viral supernatant (Black et al., 2013). Cells were washed two times with DMEM. For H3.3K4M experiments, cells were infected for 24 hr followed by a total of 72 hr of siRNA transfections or another 24 hr with plasmid overexpression. For H3.3K9M and H3.3K36M, cells were collected 48 hr post infections for analysis by FISH and western blot. For every experiment, two independent virus preparations were used for transductions. Incorporation of the histone variants into chromatin was confirmed by cellular fractionation and western blotting for the FLAG tag in the chromatin fraction.

RNA extraction and quantitative real-time PCR

Cells were washed and collected by trypsinization, followed by washing in PBS two times. Cell pellet was resuspended in Qiazol reagent (QIAGEN) and stored at −80°C before further processing. Total RNA was extracted using miRNAeasy Mini Kit (QIAGEN) with an on-column DNase digestion according to the manufacturer's instructions. RNA was quantified using NanoDrop 2000 (Thermo Scientific). Single strand cDNA was prepared using Super Script IV first strand synthesis kit (Invitrogen) using oligo dT primers or random hexamers. Expression levels were analyzed using FastStart Universal SYBR Green Master (ROX) [Roche] according to the manufacturer's instructions on a LightCycler 480 PCR machine (Roche). Samples were normalized to β-actin. Primer sequences are provided in Table S3.

Western Blotting

Cells were trypsinized and washed two times with PBS before resuspending in RIPA lysis buffer [50mM Tris pH 7.4, 150mM NaCl, 0.25% Sodium Deoxycholate, 1% NP40, 1mM EDTA, 10% Glycerol] freshly supplemented with protease inhibitor and PhosSTOP phosphatase inhibitor cocktails (Roche). Cells were lysed on ice for 15 min and stored at −80°C until further processing. Lysates were sonicated for 15 min (30sec ON and 30sec OFF cycle) at 70% amplitude in QSonica Q700 sonicator (Qsonica) followed by centrifugation at 12,000rpm for 15min. Cell lysate was transferred to a fresh tube and protein estimations were performed with Pierce BCA reagent (Thermo Scientific). Equal amounts of proteins were separated by SDS gel electrophoresis and transferred on nitrocellulose membrane (BioTrace NT, Pall Life Sciences) at 4°C for at least 3 hr at a constant current. The membranes were blocked for at least 1 hr in 5% BSA-PBST (1X PBS with 0.5% Tween-20) or 5% milk-PBST and probed over night with specific antibodies as follows at the following dilutions: anti-KDM4A (NeuromAb, 75-189) at 1:100 dilution, anti-KDM5A (ab70892, abcam) at 1:2000, anti-KDM4B (ab191434, abcam) at 1:2500, anti-H3 (ab1791) at 1:100,000, H3K4me3 (07-473, Millipore) at 1:5000, anti-GFP (73-131, NeuromAb) at 1:500, anti-FLAG HRP (A8592, Sigma) at 1:1000, anti-MCM2 (ab6153, abcam) at 1:1000, anti-MCM5 (ab6154, abcam) at 1:2000, anti-ßactin (MAB1501, Millipore) at 1:30,000, and anti-actinin (sc-17829, santacruz) at 1:2000. Membranes were washed three times in PBST the next day, incubated with goat anti-mouse IgG peroxidase conjugated secondary antibody (170-6516, Biorad) or goat anti-rabbit peroxidase conjugated secondary antibody (A00167, GenScript) at 1:2500 in 5% milk-PBST for at least 1hr at room temperature, washed 3 times with PBST and incubated in Lumi-Light western blotting substrate (12015200001, Roche) or SuperSignal West Pico PLUS Chemiluminiscent substrate (34577, ThermoScientific) for 1min. Membranes were developed with Lumi-Film Chemiluminiscent detection film (11666657001, Roche). Blocking for anti-FLAG HRP antibody was done overnight in 5%BSA-PBST before being incubated with HRP-conjugated anti-FLAG antibody, washed three times with PBST before being developed with chemiluminiscent substrate. The western blot images shown in the figures have been cropped and auto contrasted.

Cell Cycle Analyses

Asynchronous and synchronized cells were fixed and processed as performed in (Black et al., 2010). Cells were stained with 10μM EdU (Sigma) for 1 hr prior to cell cycle analyses with EdU staining. Samples were washed with PBS, centrifuged at 1400rpm for 5 min, and permeabilized with 500μL PBS containing 0.5% Triton X-100 for 30 min. Cells were washed with PBS and centrifuged at 1400rpm for 5 min. Samples were stained with 1:100 dilutions of 1mg/mL PI solution and 0.5M EDTA with 100 μg RNase A. For EdU staining, samples were stained with 125μL of EdU mixture made in 1X PBS containing 2.5μL of $CuSO_4$, 0.625μL of Alexa 647-Azide fluor and 1X reaction buffer additive present in Click-IT EdU flow cytometry kit (Life Technologies) for 1hr in dark. After EdU incubation, cells were washed once with PBS by centrifugation at 1400rpm for 5 min, followed by staining with PI solution for at least 1 hr at room temperature. Cell cycle distribution was analyzed by flow cytometer using an LSRII or Fortessa.

DNA Fluorescence *In Situ* Hybridization (FISH)

All FISH probes and associated commercial sources are noted in the key resource table. FISH probes for chromosome 1 classical satellite (1q12h), chromosome 8 centromere (alpha satellite; 8c), CDKN2C/CKS1B (referred to as 1p32.3 and 1q21.3) and chromosome X alpha satellite (Xcen) were purchased from Cytocell (Oxford Gene Technologies). Probes for 1q21.2, 1p32.3 and 1q23.3 were purchased from Agilent Technologies. The 1p32.3 (CDKN2C) probe shown alone in Figures (5E, 5G, 7C, 7D, 7H and S5H) was performed with a FISH probe purchased from Agilent Technologies (G101227R). The FISH protocol was performed as described previously in Black et al. (2013). Briefly, cell suspensions were fixed in cold methanol:glacial acetic acid (3:1) solution before being spun onto 8 Chamber Polystyrene vessel tissue culture treated glass slides (Falcon, Fisher Scientific). The slides were air-dried and incubated in 2X SSC buffer for 2 min, followed by serial ethanol dilution (70%, 85% and 100%) incubations for 2 min each, for a total of 6 min. Air-dried slides were hybridized with probes that were diluted in appropriate buffer overnight at 37°C. The slides were washed the next day in appropriate wash buffers at 69°C with 0.4X SSC for Cytocell probes or commercially available Agilent wash buffer 1 followed by washing in 2X SSC with 0.05% Tween-20 (Cytocell probes) or commercially available Agilent wash buffer 2 (Agilent probes). The slides were incubated in 1μg/mL DAPI solution made in 1% BSA-PBS, followed by a final 1X PBS wash. After the wash, the slides were mounted with ProLong Gold antifade reagent (Invitrogen).

The BAC for Xq13.1 was prepared utilizing PureLink HiPure Plasmid Filter Maxiprep kit (Life Technologies) using the recommended modified wash buffer. Probes were nick translated (Abbot Molecular Kit) in the presence of fluorescently labeled dTTP (Enzo Life Science).

FISH images were acquired using an Olympus IX81 or Olympus IX83 spinning disk microscope at 40X magnification and analyzed using Slidebook 5.0 and Slidebook 6.0 softwares. A minimum of 20 z-planes with 0.5μm step size was acquired for each field. Copy number gains for 1p32.3, 1q12h, 1q21.2, 1q21.3, 1q23.3, 1qTel, 8c, Xq13.1 and Xcen were scored in RPE cells as three or more foci. For SK-N-AS cells, 1q12h copy gain was scored for any cell with 5 or more foci, 1p32.3 copy gain was scored for any cell with 3 or more foci and 1q21.3 as 4 or more foci. For H2591, 1q12h copy gain was scored for any cell with 6 or more foci. For MDA-MB-231, 1p32.3 copy gain was scored for any cell with 5 or more foci and 1q21.3 as 7 or more foci. For MDA-MB-231 with wild-type and SET domain deletion cells, 1q12h copy gain was scored for any cell with 6 or more foci and 8c as 5 or more foci. For OVCAR5, 1p32.3 copy gain was scored for any cell with 3 or more foci and 1q21.3 as 4 or more foci. At least 100 cells were counted for each replicate of each experiment. All FISH experiments include at least two biological replicates. Representative images that are shown in the figures have been auto contrasted. Images shown in Figure 1B were acquired with the Olympus IX81 spinning disk microscope and images shown in Figures 5 and 6 were acquired with the Olympus IX83 microscope system. Extended list of probes used are provided in the key resource table.

Since we observe copy gains in a centromere-related region (i.e., 1q12h) and because centromere regions are often used as a normalizer, we decided to present the FISH results as percentage of cells with copy gains per probe instead of a ratio against a selected control region. This approach allows one to see the specificity for copy changes at each locus, while appreciating the baseline levels for regions being FISHed within and across chromosomes. Recent reports highlight the need to consider that regions in the genome of somatic and cancer cells can have different baselines and that may not be a reflection of FISH noise but a biological property of the regions (Black et al., 2015; Møller et al., 2018; Turner et al., 2017). The first experiment conducted with the probes included in the manuscript under a genetic or chemical evaluation are shown in Table S2.

Metaphase Spreads

RPE cells were seeded and treated with DMSO or KDM5-C70 inhibitor at 10uM concentration and collected after 72 hr. The cells were treated with KaryoMAX colcemid solution (GIBCO) at a final concentration of 2μg/mL for 4 hr. The cells were collected by mitotic shake off and washed with 1X PBS followed by swelling in 0.59% KCl (w/v) hypotonic solution for 1 hr 30 min. The reaction was stopped by addition of 3:1 solution of cold methanol:acetic acid, followed by 4 washes in this same fixative. The cells were then resuspended in 100μl of fixative solution. The cells were dropped on a glass slide from a height of 12-15 inches to make the metaphase spread. FISH was performed for the indicated probes post drying of the slides. The images were taken with 30 z-planes with 0.5 μm step size using the Olympus IX83 microscope. The images were analyzed for FISH using Slidebook 6.0 software.

EdU Immunofluorescence Staining

EdU staining was performed using the Click-iT EdU Alexa Fluor 488 Imaging Kit (Life Technologies) following manufacturer's protocol with minor modifications. In brief, RPE cells were plated on coverslips in 6-well plates (30,000 cells per well) and grown using standard tissue culture conditions. The cells were then transfected with two independent control and KDM5A siRNAs using Lipofectamine 3000 transfection reagent (Invitrogen) in OPTI-MEM medium (Life Technologies). The medium was changed to complete medium (DMEM) 4 hr after transfection. 52 hr after transfection, the cells were treated with a CDK1/cyclin inhibitor (Ro-3306) with a final concentration of 10 μM for 20 hr to be synchronized to late G2 phase. The cells were then labeled with EdU for a final concentration of 10 μM for 10 min before fixation with 3.7% formaldehyde in 1X PBS. The permeabilization and EdU detection steps were performed exactly as described by the manufacturer. The coverslips were mounted using VECTASHIELD HardSet Mounting Medium with DAPI (VWR) before proceeding with the imaging analysis. Data presented are the averages from two independent experiments containing two independent siRNA's each. The quantification of EdU positive cells were performed double blinded.

Cesium Chloride Density Gradient Centrifugation

RPE cells were grown and transfected with two independent KDM5A siRNA for a total of 72 hr including BrdU treatment. Cells were labeled with BrdU for 12 hr and 30 min. For GFP-control and KDM4B stably expressing cells, the cells were harvested with BrdU labeling for 12 hr and 30min for a total of 48 hr. Cells were scraped and washed twice with cold PBS and the pellet was collected by centrifugation at 1000rpm for 5min. The cell pellet was resuspended and lysed in RIPA lysis buffer [50mM Tris pH 7.4, 150mM NaCl, 0.25% Sodium Deoxycholate, 1% NP40, 1mM EDTA, 10% Glycerol] supplemented with 100μg RNase A at 37°C for 2 hr. The sample was then vortexed after adding 10% SDS and 20 μg of proteinase K and sonicated for 10sec using microprobe at 3.5 setting on Branson Sonicator to reduce viscosity. The samples were incubated at 55°C for 2 hr followed by phenol:chloroform extraction of DNA three times. DNA was ethanol precipitated overnight. The precipitated DNA was resuspended in NEB CutSmart buffer supplemented with RNase A and digested with 200U of EcoRI (NEB) and BamHI (NEB) overnight at 37°C. Digested DNA was phenol:chloroform extracted and ethanol precipitated. Pellet was resuspended in 300μL TE and incubated at 37°C for 20 min to facilitate resuspension and concentration was measured with nanodrop. Meanwhile cesium chloride (1g/mL) was dissolved in TE until reaching a refractive index of 1.4024-1.4045. 150 μg of DNA was then mixed with cesium chloride and added to the heat sealable ultracentrifuge tube (Beckman #342413, 16x76mM). The gradient was then centrifuged for 66 hr in a VTi-65 vertical ultra rotor at 44,400 rpm at 25°C under vacuum. After centrifugation, an 18 g needle was used to make an outlet at the bottom of the tube and fractions were collected in a volume of 200-300 μL for a total of around 50 fractions. DNA concentration was measured for each fraction using nanodrop. The H:H fraction was then pooled together and diluted with 2.5 to 3 times TE volume. The pooled fractions were ethanol precipitated by the addition of glycogen (Roche). The precipitated DNA was resuspended in 100μL ddwater and incubated at 37°C for 20 min to dissolve the pellet. The rereplicated samples were analyzed by qPCR on a Roche LC480 using FastStart Universal SYBR Green Master Mix ROX (Roche) following the manufacturer's instructions at 5ng DNA per well including the input DNA. Fold change was determined after normalization of each sample to the corresponding input DNA. Data presented for KDM5A rereplication are the averages using two independent siRNAs. Data presented for KDM4B are the averages from six independent replicates. Genomic regions marked in Figures 4, 6 and 7 are based on GRCh37-hg19 genome assembly.

Chromatin Immunoprecipitation (ChIP)

Sonication was performed with the Qsonica Q800R2 system (Qsonica). For KDM5A antibody ChIP, $0.3x10^6$ RPE cells were seeded in 10cm plates and transfected with control or KDM5A siRNA in lipofectamine 3000 (Life Technology) following the supplier instructions. For KDM4A, KDM4B and histone mark assessment, RPE cells were arrested in 2mM HU for 20 hr prior to cross-linking. For DNA polymerase alpha assessment, RPE cells were arrested in 10μM Ro-3306 for 20 hr prior to cross-linking. Cells were cross-linked by adding 1% formaldehyde to the media for 13 min at 37°C and stopped with 0.125M glycine, pH2.6. Plates were washed with cold PBS, and all the cells were scraped off, centrifuged at 800 rpm for 5 min at 4°C. The pellet was resuspended in cellular lysis buffer (5mM PIPES pH8.00, 85mM KCl, 0.5% NP40) supplemented with protease and phosphatase inhibitors, incubated 5min on ice and centrifuged at 800 rpm, 5 min at 4°C. The pellet was resuspended in nuclear lysis buffer (NLB, 50mM Tris, pH 8.0, 10mM EDTA, 0.2% or 1.0% SDS). All histone ChIPs were carried out with chromatin made in NLB with 1.0% SDS and others in NLB containing 0.2% SDS. Chromatin was resuspended in NLB-1.0% SDS and were then sonicated at 70% amplitude 15 s on 45sec off setting for 35 min and NLB-0.2%SDS for 45 min. 4 μL of chromatin was reverse cross-linked overnight at 65°C in presence of proteinase K. After RNase treatment, DNA was isolated with phenol:chloroform extraction and checked on 1% agarose gel for a smear below 300bp. 1-10 μg of chromatin was precleared by centrifugation at 14,000rpm for 10min at 4°C. For each IP, chromatin was immunoprecipitated with 2μg of antibody in dilution IP buffer (16.7mM Tris pH 8.0, 1.2mM EDTA pH 8.0, 167mM NaCl, 0.2% SDS, 0.24% or 1.84% Triston-X-100) at 4°C overnight. Chromatin was precleared for 2 hr each with protein A agarose and magnetic protein A or protein G beads (Invitrogen; to match antibody isotype) before immunoprecipitation. The immunoprecipitated material was washed 2 times in dilution IP buffer, 1 time in TSE buffer (20mM Tris pH 8.0, 2mM EDTA pH8.0, 500mM NaCl, 1% Triton X-100, 0.1% SDS), 1 time in LiCl buffer (100mM Tris pH 8.0, 500mM LiCl, 1% deoxycholic acid, 1% NP40) and 2 times in TE (10mM Tris pH 8.0, 1mM EDTA pH8.0) before elution in elution buffer (50mM NaHCO3, 140mM NaCl, 1% SDS) with 10ug proteinase K at 1 hr 55°C 1000 rpm. The samples were removed from beads and reverse cross-linked at 65°C for 4 hr. Immunoprecipitated DNA

was purified using either PCR purification columns (Promega) or AMPureXP beads. Antibodies used for ChIP are as follows: KDM5A (abcam ab70892; chromatin was treated with 200μg of RNase A before IP), KDM5A (Bethyl A300-897A; chromatin was treated with 200μg of RNase A before IP), KDM4A (P006, Structural Genomic Consortium; chromatin was treated with 200μg of RNase A before IP), KDM4A (P014, Structural Genomic Consortium; chromatin was treated with 200μg of RNase A before IP), KDM4B (abcam ab191434; chromatin was treated with 200μg of RNase A before IP), H3K4me3 (Millipore 07-473), H3 (abcam ab1791), Polymerase alpha (ab31777-100; chromatin was treated with 200μg of RNase A before IP) and H3K36me3 (Abcam, ab9050). For KDM5A ChIP, data presented are the averages from two independent siRNAs using two different KDM5A antibody. For Polymerase alpha and H3K4me3 ChIP's, data presented are the averages from six replicates. For KDM4A ChIP, data presented are the averages from eight replicates with two antibodies. For KDM4B ChIP, data presented are the averages from two independent cell lines. For H3K36me3 ChIP, data presented are the averages from four replicates. All the ChIPs were performed with at least two independent chromatin preparations from two independent siRNAs or two independently made RPE cell lines.

Cell Fractionation

Cytoplasmic, nuclear and chromatin fractions were prepared from RPE cells. Cell pellets were washed twice in ice cold PBS and resuspended in ice cold hypotonic buffer (10mM HEPES pH 7.9, 10mM KCl, 0.1M EDTA, 0.5M EGTA) and incubated on ice for 15 min. Swollen cells were lysed by addition of NP-40 to 10% with 10 s of vortexing. Lysed cells were centrifuged and the supernatant kept as cytoplasm. The nuclear pellet was resuspended in high salt buffer (10mM HEPES pH 7.9, 400mM NaCl, 1mM EDTA, 5mM EGTA) and incubated at 4°C for 15min with rotation. Extracts were centrifuged and the supernatant was kept as nuclear extract. The pellets were resuspended in N-Buffer (20mM Trish pH 7.5, 100mM KCl, 2mM MgCl2, 1mM CaCl2, 0.3M Sucrose, 0.1% Triton X-100, 3U per mL micrococcal nuclease). Samples were sonicated for 15 min at 70% amplitude in a Q700 cup horn (QSonica) and then incubated at room temperature for 15 min for MNase digestion. Reactions were stopped by addition of 5mM EDTA and centrifuged to clear. Supernatant was kept as chromatin extract.

HaloTag Mammalian Pulldown for Mass spectrometry

HEK293T cells (12×10^6 cells) were transfected with the N-terminal HaloTag-KDM4B fusion (O94953) or the control HaloTag alone plasmid (Promega G6591) using FuGENE HD Transfection Reagent (Promega E2311). Twenty four hr post-transfection, cells were lysed in mammalian lysis buffer (50mM Tris-HCl, pH 7.5, 150mM NaCl, 1% Triton X-100, and 0.1% sodium deoxycholate) including protease Inhibitor cocktail and RQ1 RNase-Free DNase (Promega G6509) for 10min on ice. Using a syringe, lysates was homogenized and then further clarified by centrifugation at 14.000 x g for 5min. The resultant supernatants were incubated with HaloLink Resin (Promega G6509) that had been pre-equilibrated in TBS and 0.05% IGEPAL CA-640 (Sigma) for 15 min at 22°C with rotation. HaloTag pulldown complexes bound to resin were washed 5 times with wash buffer (Promega G6509), and protein interactors were eluted with SDS elution buffer (50mM Tris-HCl, pH 7.5, and 1% SDS). Eluted purified complexes were subjected to trypsin (Promega) gel digestion for 4 hr and then analyzed directly by nano LC/MS/MS with a NanoAcquity HPLC (Waters) interfaced with an Orbitrap Velos Pro (Thermo Scientific) tandem mass spectrometer by MS Bioworks, LLC (Ann Arbor, Michigan). A list of interactors is presented in Table S4.

Immunoprecipitation

Immunoprecipitation was carried out as described previously in (Van Rechem et al., 2011; Van Rechem et al., 2015). In brief, HU arrested HEK293T cells (2mM HU for 20 hr) were washed with cold PBS before being spun down. To obtain nuclei enriched extracts, the cell pellet was resuspended in cellular lysis buffer (5 mM PIPES pH8, 85 mM KCl, 0.5% NP40, protease and phosphatase inhibitors) and incubated 5 min on ice before being spun down. The pellet was lysed in IPH buffer (50mM Tris-HCl, pH 8.0, 150mM NaCl, 5mM EDTA, 0.5% NP-40 and 10% glycerol, protease and phosphatase inhibitors) and sonicated with a probe (Branson Sonifier 450) for 25sec. The lysate was then cleared by centrifugation at 4°C full speed for 10 min and quantified using Pierce BCA protein assay. For immunoprecipitation, 500ug of lysate was incubated overnight on a rotator at 4°C in 1mL of IPH buffer with 25μL of Dynabeads Protein A (Invitrogen 10002D), 2 μg of KDM4B antibody (ab191434, abcam) or rabbit IgG, and 100 μg/mL ethidium bromide. The beads were then washed five times in 1mL of IPH buffer with vortexing between each wash, resuspended in SDS sample loading buffer and heated at 95°C for 10min before being processed for western blot and probed for MCM2 (ab6153) and MCM5 (ab6154).

NanoBRET assays

HEK293 cells (4×10^5) were plated in each well of a 12-well plate and co-transfected with various NanoLuc donor and HaloTag acceptor pairs including; HaloTag-MCM3 (P25205), HaloTag-MCM4 (P33991), HaloTag-MCM5 (P33992), HaloTag-MCM7 (P33993), HaloTag-POLA2 (Q14181), HaloTag-POLD1 (P28340), NanoLuc-KDM4A (O75164), NanoLuc-KDM4B (O94953) or HaloTag alone (Promega G6591). All HaloTag and NanoLuc fusion vectors utilized pFN21A and pFN31K backbones respectively (Promega) and were transfected at 1:100-fold dilution (2μg HaloTag acceptor: 0.02ug NL donor) or in varying ratios of 1:100, 33.3, 11.1, 3.7, 1.2, 0.41, 0.14, 0.046, and 0 for donor saturation assays. 20 hr post-transfection cells were collected, washed with PBS, and exchanged into phenol red-free Opti-MEM in the absence (control sample) or the presence (experimental sample) of 100 nM NanoBRET 618 fluorescent ligand (Promega). Cell density was adjusted to 2×10^5 cells/ml and then re-plated in a 96-well assay white plate (Corning Costar #3917) and let recover for 20 hr at 37°C in the presence of 5% CO_2. NanoBRET furimazine

substrate (Promega) was added to both control and experimental samples at a final concentration of 10 μM. Readings were performed within 5 min using the GloMax Discover (Promega) equipped with NanoBRET 450/8 nm bandpass and 600 nm longpass filters with a 0.3 s reading setting. A corrected BRET ratio was calculated and is defined as the ratio of the emission at 600 nm/450 nm for experimental samples (i.e., those treated with NanoBRET fluorescent ligand) subtracted by the emission at 600 nm/450 nm for control samples (not treated with NanoBRET fluorescent ligand). BRET ratios are expressed as milliBRET units (mBU), where 1 mBU corresponds to the corrected BRET ratio multiplied by 1000. Data presented are the averages from quandruplicates. For NanoBRET assay showing decreased interaction of KDM4B with Histone H2B or H4 in RPE cells containing a K4M mutant H3.3, the wild-type or H3.3 K4M mutant RPE cells were co-transfected with NanoLuc-KDM4B in combination with either H2B-HaloTag or H4-HaloTag. Data presented are the graphs of corrected BRET ratios for KDM4B/H2B or KDM4B/H4 with four independent replicates.

Drug Treatment Conditions

For cell cycle enrichment experiments: cells were synchronized in G1/S using hydroxyurea (HU; Sigma) at 2mM final concentration for 20 hr in RPE. Cells were released from HU by washing two times with fresh media followed by culturing in complete media for the indicated time points. Synchronization at G2/M was performed with Ro-3306 [Enzo LifeSciences; (Black et al., 2013)] at 10μM final concentration for 20 hr. KDM5-C70 was purchased from Xcessbio [Fisher Scientific; (Johansson et al., 2016)] and treated at the indicated concentrations for 48 hr or 72 hr. For KDM5-C70/release experiment: cells were treated with KDM5-C70 at 10μM final concentration for 48 hr, followed by no wash off and a 24 hr drug wash off with fresh media. All the cells were collected 72 hr post drug treatment (Figures 2B and 2C). For Figures 2E and 2F, cells were treated with HU at 2mM final concentration for 20 hr. Vehicle or KDM5-C70 at 10μM final concentration was added for 24 hr followed by a no wash off or a 6 hr wash off with fresh media.

For siRNA/drug experiments, cells were transfected with two independent KDM5A siRNAs in OPTI-MEM medium for 4 hr, followed by change to complete media. DMSO or Ro-3306 at 10μM final concentration was added during the last 20 hr of a total of 72 hr collection (Figure 2J). For Figures 3D and 7C, cells were transfected with KDM4A and KDM4B siRNAs in OPTI-MEM medium for 4 hr, followed by change to complete media with the addition of KDM5-C70 at 10μM final concentration. Cells were harvested after 72 hr from transfection. The FISH counting was done double blinded for at least two biological replicates for Figures 3D and 7C.

For the cisplatin drug experiments in Figures S7T and S7U, S7W and S7Y, 5000 cells for MDA-MB-231, OVCAR5 and SK-N-AS were seeded in 24-wells in 500μL total media. 24 hr post seeding, the cells were treated with 1uM of KDM5-C70. After 24 hr of KDM5-C70 treatment, cells were treated with either 1uM or 3uM cisplatin for 48 hr. Cells were trypsinized and were counted after trypan blue addition and represented in the graphs normalized to their respective vehicle treatment. Five independent experiments for each cell line were performed in triplicate.

QUANTIFICATION AND STATISTICAL ANALYSIS

Analysis of Mass Spectrometry Data

Halo tag-purified KDM4B complexes were analyzed and processed by MS Bioworks, LLC (Ann Arbor, Michigan) and performed as exactly described in (Black et al., 2013). Data were searched with Mascot (Matrix Science) against the concatenated forward/decoy UniProt Human Database. Mascot DAT files were visualized and filtered by Scaffold (Proteome Software). A minimum protein value of 90% was used as a filter. A minimum peptide value of 50% (Protein and Peptide Prophet scores) and at least two unique peptides per protein were required. Spectral counting was performed and normalized spectral abundance factors determined. The data reported has less than 1% false discovery rate (FDR) at the protein level based on counting the number of forward and decoy matches. A list of the peptides can be found in Table S4.

Statistical Analysis

All pairwise comparisons were done using two-tailed Student's t test unless otherwise stated. Significance was determined if the p value was < 0.05. All FISH experiments were carried out with at least two independent siRNAs unless otherwise stated and at least 100 nuclei per replicate per experiment were counted for all the FISH studies conducted. All error bars represent the SEM. Experiments that have been counted double blinded have been noted in the methods.

Cell

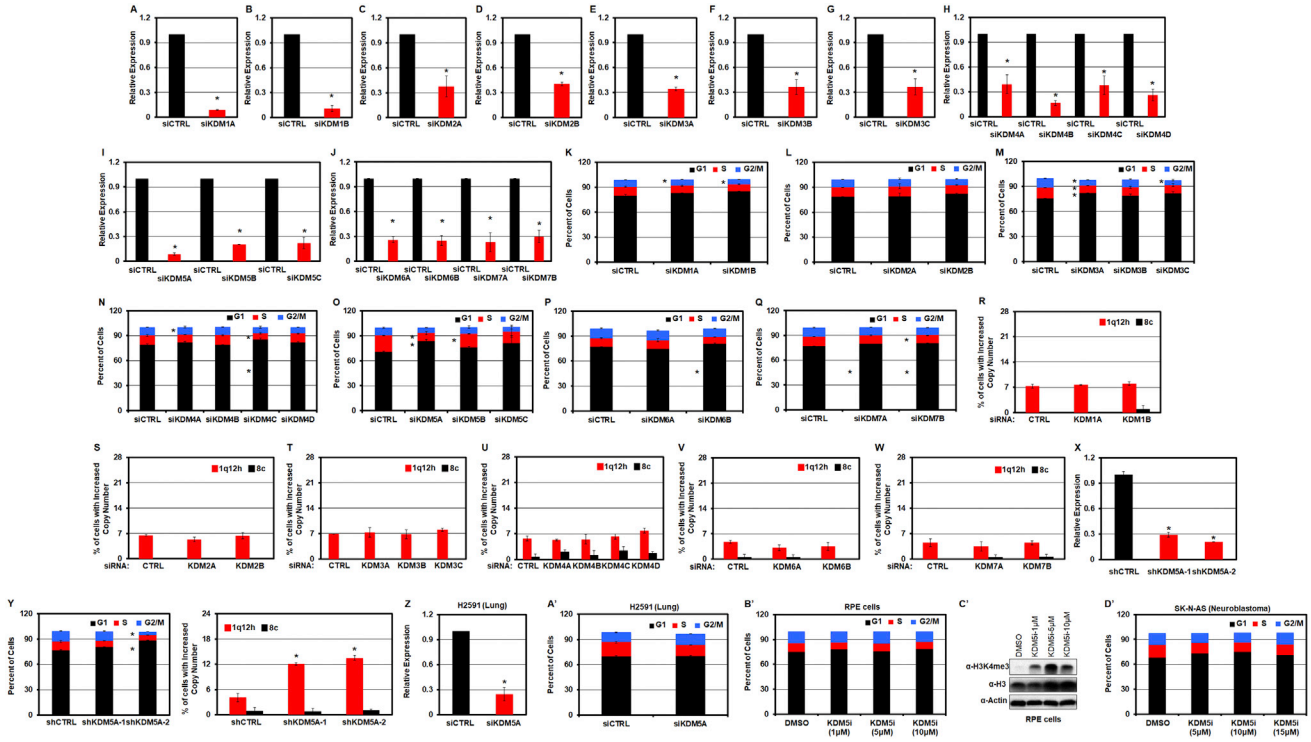

Figure S1. KDM5A Inhibition Promotes Site-Specific Copy Gains, Related to Figure 1

(A-J) qPCR analysis was performed to validate specific gene knockdowns of KDM1-7 family.

(K-Q) FACS analysis was performed on KDM family members after 72h of knockdown.

(R-W) FISH was performed in RPE cells depleted for each KDM: KDM1 (R), KDM2 (S), KDM3 (T), KDM4 (U), KDM6 (V) and KDM7 (W) for chromosome 1q12h and chromosome 8 centromere (8c). The FISH counting for panels V and W were done double blinded for at least one set of experiments.

(X) qPCR analysis was performed to validate KDM5A knockdown in two different KDM5A shRNA cell populations (shRNA-1 and shRNA-2).

(Y) FACS was performed on two different KDM5A shRNA cell populations (shRNA-1 and shRNA-2). DNA FISH showed a significant increase in 1q12h copy gains upon KDM5A shRNA transduction (shRNA-1 and shRNA-2) compared to the control shRNA. The FISH counting were done double blinded for at least one set of shRNA.

(Z) qPCR analysis was performed to validate KDM5A siRNA knockdowns in H2591 lung cancer cells.

(A') FACS analysis was performed in control and KDM5A siRNA knockdowns in H2591 lung cancer cells.

(B') FACS analysis was performed on one set of RPE cells treated with KDM5-C70 inhibitor treatment at three different concentrations for 72hr.

(C') western blots for H3K4me3, H3 and β-actin in DMSO and KDM5 inhibitor concentration treatments after 72hr were performed.

(D') FACS analysis was performed on one set of SK-N-AS cells treated with KDM5 inhibitor at three different concentrations for 48hr.

Error bars represent the SEM. Any significant differences ($p < 0.05$) are indicated with an asterisk by two-tailed Student's t- test.

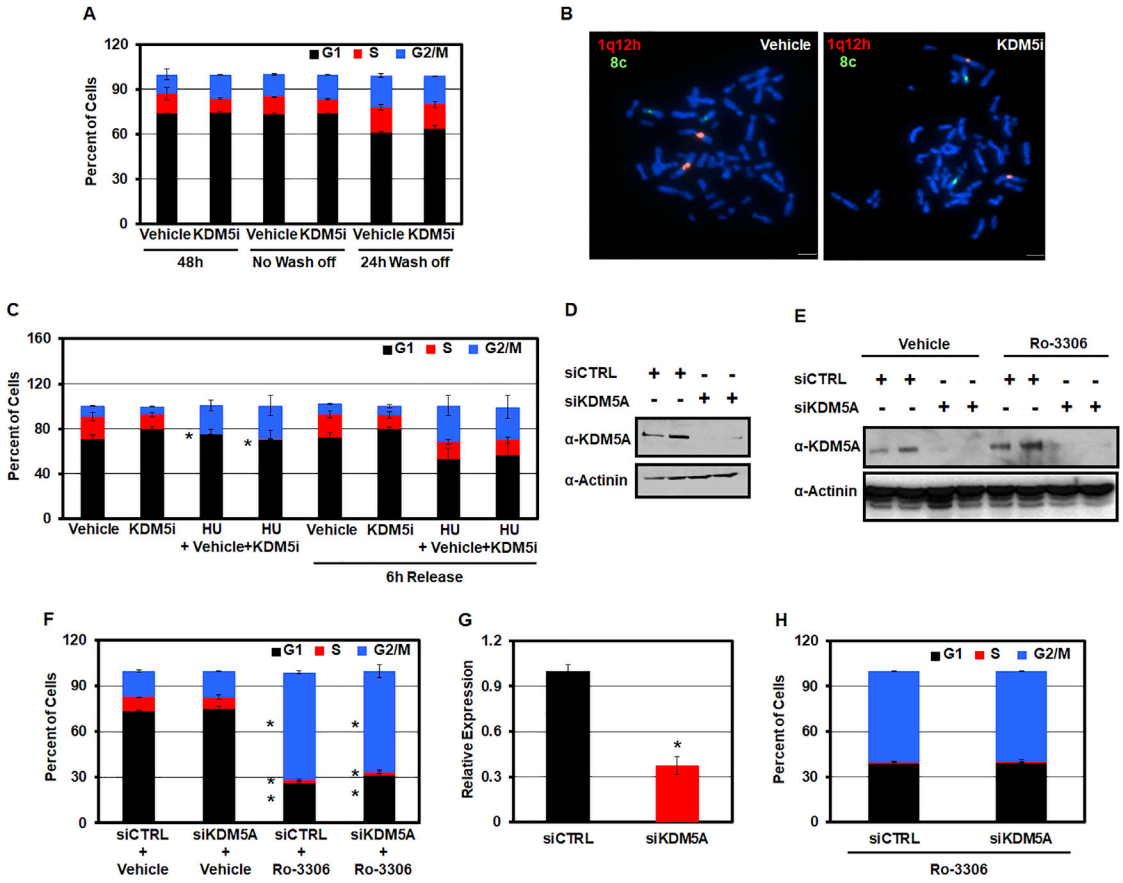

Figure S2. KDM5A-Associated Site-Specific Copy Gains Are Transient, Require S Phase, and Are Rereplicated, Related to Figure 2

(A) FACS was performed on the vehicle and KDM5-C70 treated cells after 48hr and with and without 24hr of drug wash-off.

(B) Example metaphase spreads for 1q12h (red) and 8c (green) regions in vehicle and KDM5-C70 treated cells are shown. Scale bars represent 5 μm.

(C) FACS analysis of samples treated with HU and KDM5 inhibitor are shown. Samples were released from HU after 6hr.

(D) western blot shows decreased KDM5A protein levels compared to controls using two different siRNAs in RPE cells used for the rereplication assay.

(E) western blot showed decreased KDM5A protein level using two different siRNAs in samples treated with vehicle (DMSO) and CDK1 inhibitor (Ro-3306) for 20hr. Actinin is used as a loading control.

(F) FACS analysis was performed on KDM5A siRNA treated samples with and without Ro-3306 treatment.

(G) qPCR analysis was performed to validate KDM5A knockdown in RPE cells. Error bars represent the SEM from four replicates.

(H) FACS analysis was performed on control and KDM5A siRNA treated RPE cells after Ro-3306 treatment. Error bars represent the SEM. Any significant differences ($p < 0.05$) are indicated with an asterisk by two-tailed Student's t- test.

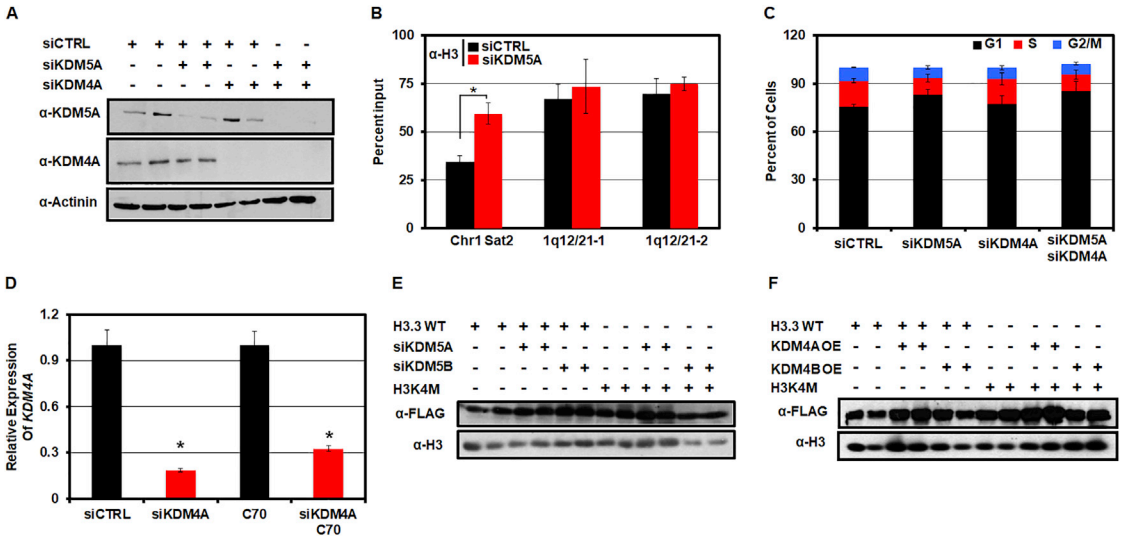

Figure S3. KDM5A Depletion Promotes H3K4me3 and KDM4A Recruitment at Copy-Gained Loci, Related to Figure 3

(A) western blot shows decreased KDM5A and KDM4A protein level in samples treated with KDM4A siRNAs, KDM5A siRNAs and both KDM4/5 siRNAs for 72hr. Actinin is used as a loading control.

(B) Quantification of histone H3 with ChIP qPCR in control and KDM5A knockdown samples at chromosome 1 sat2 (Chr1 sat2) and two different genomic coordinates [1q12/21-1 (chr1: 142,704,000) and 1q12/21-2 (chr1: 142,706,000)]. Error bars represent the SEM from six replicates.

(C) FACS analysis was performed on samples with KDM4A siRNA, KDM5A siRNA and both after 72hr of knockdown.

(D) qPCR analysis for KDM4A was performed on control and KDM4A siRNA transfected cells with vehicle and KDM5-C70 inhibitor treatment after 72hr. Error bars represent the SEM from four replicates.

(E) western blot for FLAG incorporation and histone H3 in chromatin fractions with KDM5A and KDM5B knockdown transduced with either the H3 wild-type (H3.3 WT) or the H3 lysine 4 to methionine (H3K4M) mutant.

(F) western blot for FLAG incorporation and histone H3 in chromatin fractions with KDM4A and KDM4B overexpression after transduction with either H3 wild-type or H3K4M was performed. Any significant differences ($p < 0.05$) are indicated with an asterisk by two-tailed Student's t test.

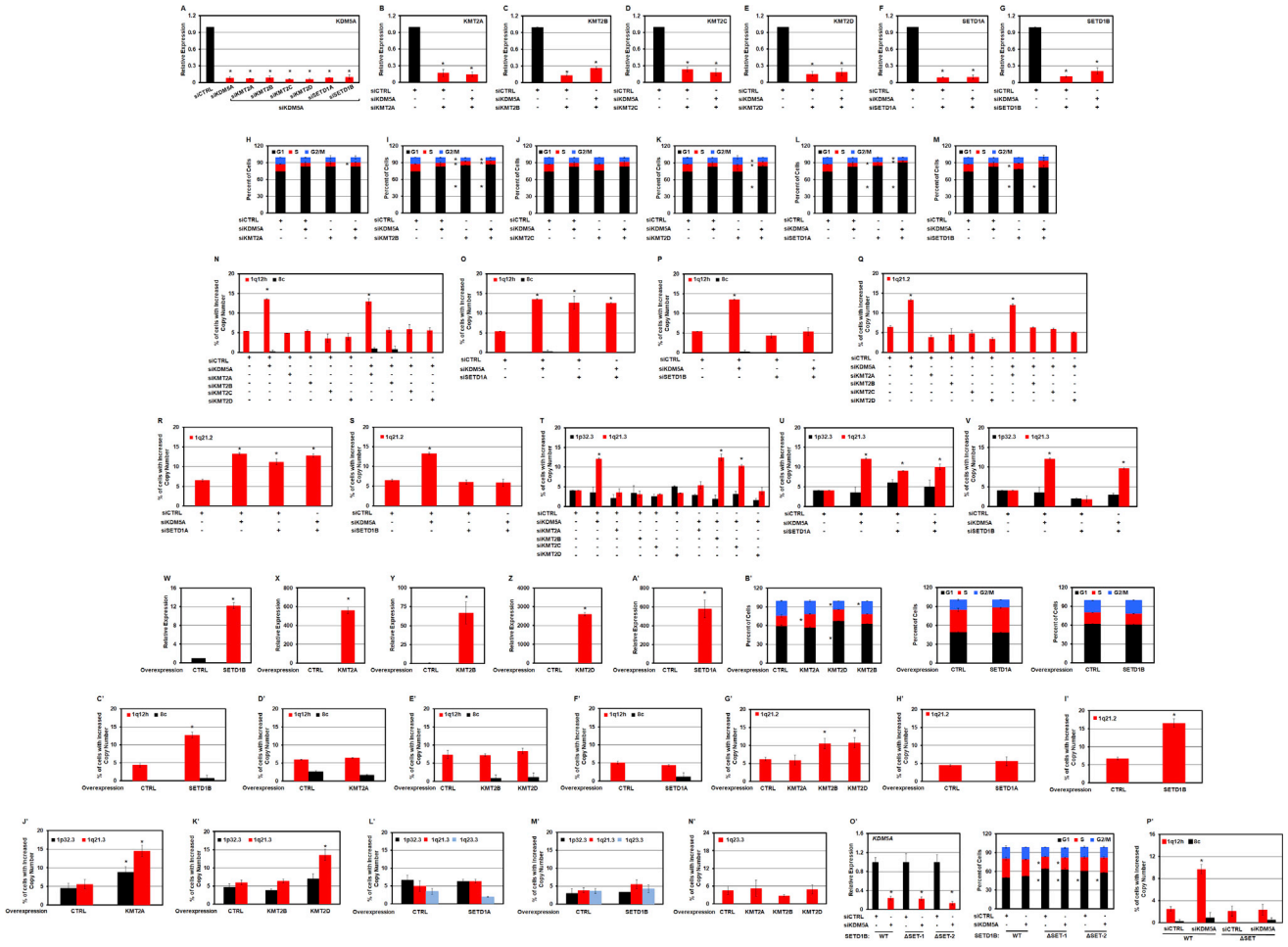

Figure S4. Site-Specific Copy Gains Are H3K4 KMT-Dependent, Related to Figure 4

(A-G) qPCR analysis was performed to validate specific gene knockdowns.

(H-M) FACS analysis was performed on samples with KDM5A, H3K4 methyltransferase (KMT2A, KMT2B, KMT2C, KMT2D, SETD1A and SETD1B) or KDM5A/KMT depletions after 72hr of knockdown. The same control and KDM5A siRNA profiles are used in each of the corresponding graphs so a comparison to the individual KMT and co-depletions can be seen relative to the control and siKDM5A conducted across the same experiment.

(N-V) Quantification of DNA FISH from cells depleted for KDM5A, H3K4 KMTs or KDM5A/KMT: 1q12h and 8c (N-P), 1q21.2 (Q-S), 1p32.3 and 1q21.3 (T-V).

(W-A') qPCR analysis was performed to validate specific KMT gene overexpression.

(B') FACS analyses were performed on cells overexpressing the KMTs.

(C'-N') Quantification of DNA FISH from cells overexpressing KMTs: 1q12h and 8c (C'-F'), 1q21.2 (G'-I'), 1p32.3 and 1q21.3 (J'-M') and 1q23.3 (N').

(O') qPCR analysis was performed to validate KDM5A knockdowns in wild-type (WT) and SETD1B SET domain deletions (ΔSET-1 and −2) in MDA-MB-231 cells. FACS analyses were performed on control and KDM5A knockdowns in wild-type (WT) and SET domain deletions (ΔSET-1 and 2) in MDA-MB-231 cells.

(P') FISH for 1q12h and 8c was performed in wild-type (WT) and ΔSET-1 and 2 in MDA-MB-231 cells. The graph presented shows combined values for both the SET domain deletions (ΔSET-1 and 2).

Error bars represent the SEM. At least one set of DNA FISH for panels N-V was counted double blinded. *represents $p < 0.05$ (Student's t test).

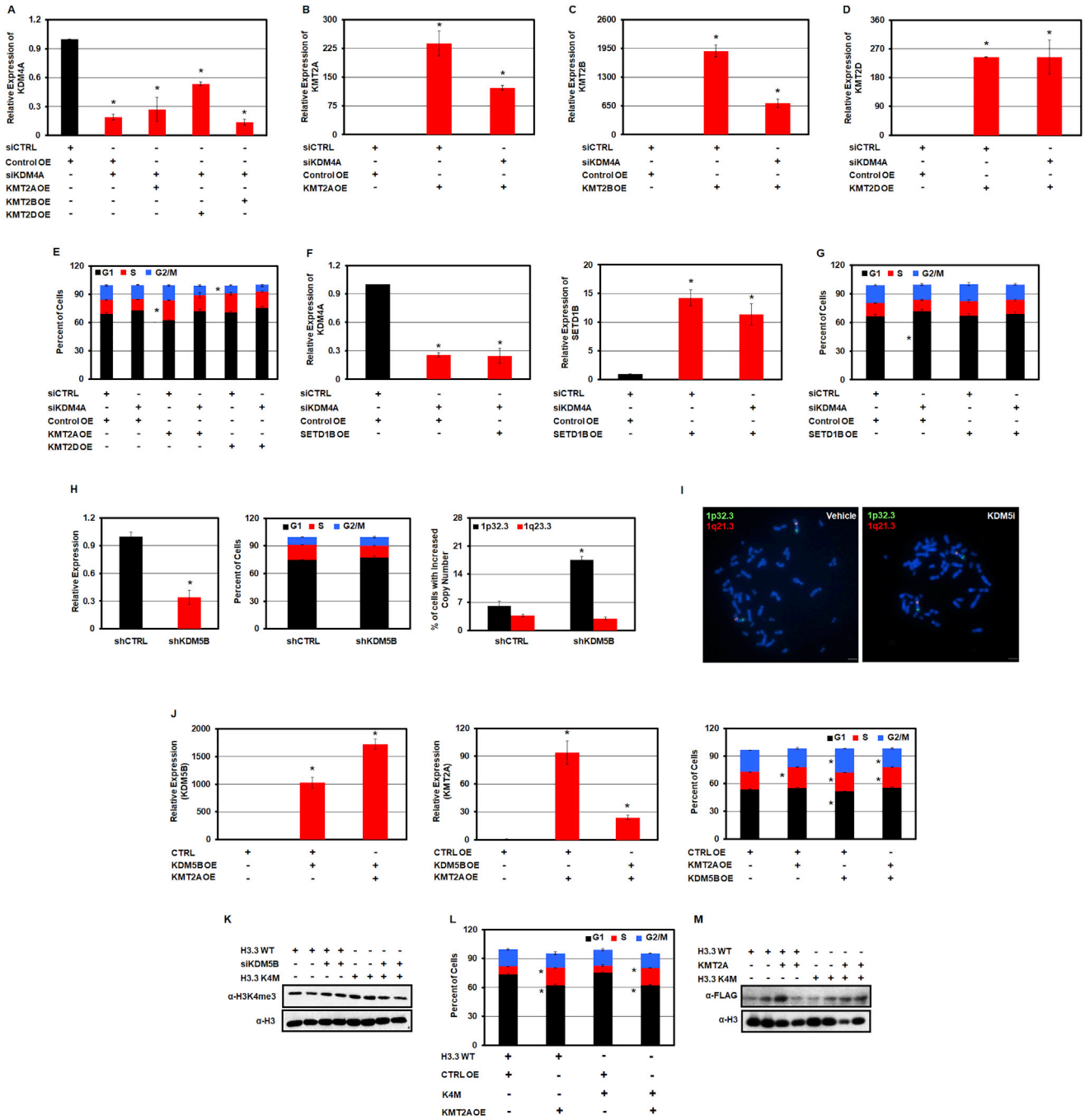

Figure S5. Site-Specific Copy Gains Are H3K4 KMT Dependent and KDM5B Regulates the 1p32.3 TSSG, Related to Figures 4 and 5

(A-D) qPCR analysis was performed to validate KDM4A gene knockdown and KMT overexpression.

(E) FACS analysis was performed on samples with KDM4A gene knockdown and KMT overexpression.

(F) qPCR analysis was performed to validate KDM4A depletion and SETD1B overexpression.

(G) FACS analysis was performed on samples with KDM4A knockdown and SETD1B overexpression.

(H) qPCR, FACS and DNA FISH analyses for 1p32.3 and 1q23.3 was performed on four replicate experiments from RPE cells transduced with a single shRNA against KDM5B.

(I) Example metaphase spreads followed by DNA FISH for 1p32.3 (green) and 1q21.3 (red) was performed in vehicle and KDM5-C70 treated RPE cells. Scale bars represent 5 μm.

(J) qPCR and FACS analyses were performed to validate KMT2A and KDM5B overexpressing cells.

(legend continued on next page)

(K) western blot for H3K4me3 and histone H3 was performed in samples from control and KDM5B knockdown cells transduced with H3.3WT and H3.3K4M.
(L) FACS was done in samples with control and KMT2A overexpression transduced with H3.3WT and H3.3K4M.
(M) western blot for FLAG and histone H3 was conducted on samples with control and KMT2A overexpression that were transduced with H3.3WT and H3.3K4M.
Error bars represent the SEM. Any significant differences ($p < 0.05$) are indicated with an asterisk by two-tailed Student's t test.

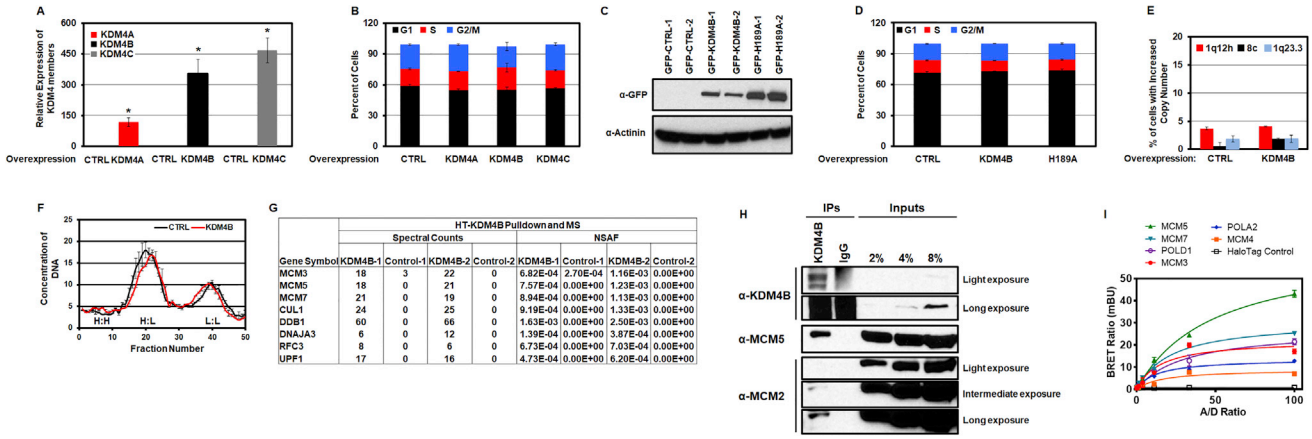

	HT-KDM4B Pulldown and MS							
	Spectral Counts				NSAF			
Gene Symbol	KDM4B-1	Control-1	KDM4B-2	Control-2	KDM4B-1	Control-1	KDM4B-2	Control-2
MCM3	18	3	22	0	6.82E-04	2.70E-04	1.16E-03	0.00E+00
MCM5	18	0	21	0	7.57E-04	0.00E+00	1.23E-03	0.00E+00
MCM7	21	0	19	0	8.94E-04	0.00E+00	1.13E-03	0.00E+00
CUL1	24	0	25	0	9.19E-04	0.00E+00	1.33E-03	0.00E+00
DDB1	60	0	66	0	1.63E-03	0.00E+00	2.50E-03	0.00E+00
DNAJA3	6	0	12	0	1.39E-04	0.00E+00	3.87E-04	0.00E+00
RFC3	8	0	6	0	6.73E-04	0.00E+00	7.03E-04	0.00E+00
UPF1	17	0	16	0	4.73E-04	0.00E+00	6.20E-04	0.00E+00

Figure S6. KDM4B Promotes Site-Specific Copy Gains and Rereplication at 1p32.3, Related to Figure 6

(A) qPCR was used to validate KDM4 overexpression.

(B) FACS is shown for samples with KDM4 overexpression.

(C) western blot for GFP demonstrated RPE cells stably overexpress KDM4B and the KDM4B with the H189A mutation.

(D) FACS for RPE cells that stably overexpress KDM4B and the KDM4B with the H189A mutation.

(E) DNA FISH analyses for 1q12h, 8c and 1q23.3 was performed in control and KDM4B stably expressing RPE cells.

(F) Graph with the concentration of DNA determined by nanodrop is shown for control and KDM4B stably overexpressing cells. The graph represents heavy-heavy (H:H), heavy-light (H:L) and light-light (L:L) peaks of the fractionated gradients.

(G) Mass spectrophotometry analyses of KDM4B interacting proteins are shown in the Table with peptide counts and NSAF values. List of interactors are in Table S4.

(H) Co-immunoprecipitation was done with endogenous KDM4B protein and the corresponding replication proteins: MCM2 and MCM5. Various exposures are shown after autocontrast.

(I) NanoBRET donor saturation assay showing the specificity of the *in vivo* interaction of KDM4B with MCM3, MCM4, MCM5, MCM7, POLA2, and POLD1. HEK293 cells were co-transfected with a fixed low level of NanoLuc-KDM4B in the presence of increasing amounts of acceptor DNA of HaloTag-MCM3, HaloTag-MCM4, HaloTag-MCM5, HaloTag-MCM7, HaloTag-POLA2, HaloTag-POLD1, or HaloTag alone (negative control).

Error bars represent the SEM. Any significant differences ($p < 0.05$) are indicated with an asterisk by two-tailed Student's t test.

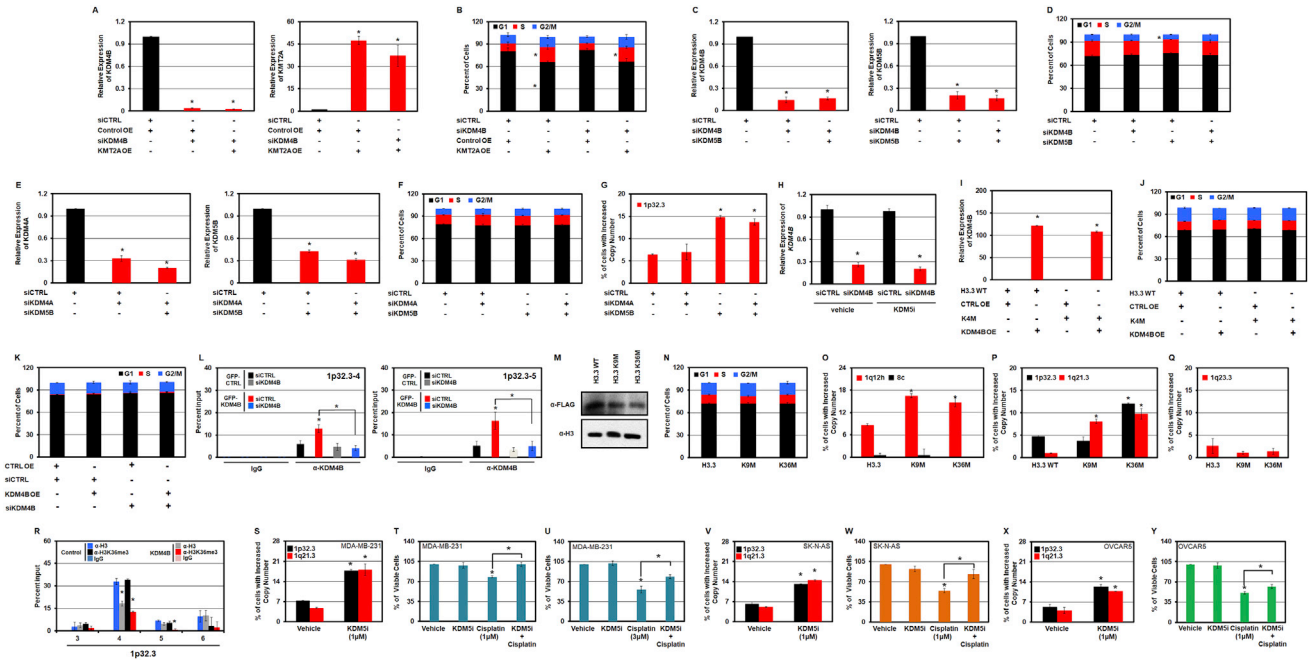

Figure S7. 1p32.3 TSSG Formation Correlated with KDM4B Recruitment and Reduced H3K36me3, Related to Figure 7

(A) qPCR analysis was performed to validate KDM4B knockdown and KMT2A overexpression.

(B) FACS analysis was performed on samples with KDM4B depletion and KMT2A overexpression.

(C) qPCR analysis was performed on samples with sequential knockdown of KDM4B followed by 48hr of KDM5B knockdown.

(D) FACS analysis was performed on samples with sequential knockdown of KDM4B followed by 48hr of KDM5B knockdown.

(E) qPCR analysis was performed on samples with sequential knockdown of KDM4A followed by 48hr of KDM5B knockdown.

(F) FACS analysis was performed on samples with sequential knockdown of KDM4A followed by 48hr of KDM5B knockdown.

(G) FISH for 1p32.3 locus (Agilent Probe) was performed on samples with sequential knockdown of KDM4A followed by 48hr of KDM5B knockdown.

(H) qPCR analysis for KDM4B was performed on control and KDM4B siRNA transfected cells with vehicle and KDM5-C70 inhibitor treatment after 72hr.

(I) qPCR analysis was performed in samples with KDM4B overexpression in H3.3WT and H3.3K4M transduced cells.

(J) FACS analysis was performed on samples in (I).

(K) FACS for HU treated cells in GFP-control and GFP-KDM4B cells transfected with control and KDM4B siRNAs. These samples were used for ChIP.

(L) ChIP qPCR for KDM4B in control and GFP-KDM4B cells transfected with control and KDM4B siRNA was performed at two different genomic regions that showed rereplication and are labeled as 1p32.3-4 and 1p32.3-5. Error bars represent the SEM from four replicates.

(M) western blot for FLAG incorporation in H3.3 wild-type, H3.3K9M and H3.3K36M mutations are shown.

(N) FACS for RPE cells transduced with H3.3 wild-type, H3.3K9M and H3.3K36M.

(O-Q) DNA FISH analyses for 1q12h, 8c, 1p32.3, 1q21.3 and 1q23.3 were performed in cells transduced with H3.3 wild-type, H3.3K9M and H3.3K36M.

(R) ChIP qPCR for H3 and H3K36me3 antibodies in control and GFP-KDM4B cells was performed. Error bars represent the SEM from four replicates. The ratios are shown in Figure 7I.

(S) DNA FISH analyses for 1p32.3 and 1q21.3 was performed after vehicle and KDM5-C70 treatment in MDA-MB-231 cells. At least one set of DNA FISH was counted double blinded.

(T and U) MDA-MB-231 cells were seeded and pre-treated with KDM5-C70 (1μM) for 24h followed by cisplatin treatment (1μM and 3μM) for 48h. Cells were stained with trypan blue and non-trypan blue cells were counted and presented normalized to the vehicle. The numbers represent the average values from 5 independent experiments done in triplicate wells.

(V) DNA FISH analyses for 1p32.3 and 1q21.3 was performed after vehicle and KDM5-C70 treatment in SK-N-AS cells. At least one set of DNA FISH was counted double blinded.

(W) SK-N-AS cells were seeded and pre-treated with KDM5-C70 (1μM) for 24h followed by cisplatin treatment (1μM) for 48h. Cells were stained with trypan blue and non-trypan blue cells were counted and presented normalized to the vehicle. The numbers represent the average values from 5 independent experiments done in triplicate wells.

(X) DNA FISH analyses for 1p32.3 and 1q21.3 was performed after vehicle and KDM5-C70 treatment in OVCAR5 cells. At least one set of DNA FISH was counted double blinded.

(Y) OVCAR5 cells were seeded and pre-treated with KDM5-C70 (1μM) for 24h followed by cisplatin treatment (1μM) for 48h. Cells were stained with trypan blue and non-trypan blue cells were counted andand presented normalized to the vehicle. The numbers represent the average values from 5 independent experiments done in triplicate wells.

Error bars represent the SEM. Any significant differences ($p < 0.05$) are indicated with an asterisk by two-tailed Student's t test.